THE ASTROPHYSICAL JOURNAL, 341:246–269, 1989 June 1

THE INFRARED EMISSION BANDS. III. SOUTHERN *IRAS*[1] SOURCES

MARTIN COHEN
Radio Astronomy Laboratory, University of California, Berkeley
A. G. G. M. TIELENS
Space Sciences Laboratory, University of California, Berkeley
JESSE BREGMAN AND FRED C. WITTEBORN
Astrophysical Experiments Branch, NASA-Ames Research Center
DAVID M. RANK
Lick Observatory, University of California, Santa Cruz
L. J. ALLAMANDOLA and DIANE H. WOODEN
Astrophysical Experiments Branch, NASA-Ames Research Center
AND
M. DE MUIZON
Leiden Observatory, Leiden University, and Observatoire de Paris, Section de Meudon
Received 1988 July 25; accepted 1988 November 2

ABSTRACT

We present airborne 5–8 μm spectra of southern *IRAS* sources which reveal strong polycyclic aromatic hydrocarbon (PAH) emission features. The good correlation between the bands, in particular the dominant 6.2 and "7.7" μm features, strongly imply a common carrier, reinforcing the PAH hypothesis. However, small but detectable spectral variations exist. Planetaries have a distinctly different ratio of $I(6.2)/I(7.7)$ than other nebulae, accompanied by a redward shift in the actual wavelength of the "7.7" μm peak. Further, we have detected a new feature, previously predicted from laboratory spectra of PAH molecules, at 5.2 μm in many of these sources. Spectra of two rare [WC 10] planetary nebula nuclei indicate a very prominent plateau of emission, linking the 6.2 and 7.7 μm bands. Several of our sources show definite evidence for emission structure between 14 and 23 μm in their *IRAS Low-Resolution Spectral Atlas* spectra: we attribute this structure to PAH bands, too.

We have defined the "generic" spectrum of emission bands relating the mean intensities of each band to that of the strongest, near 7.7 μm. We have added three more planetary or protoplanetary nebulae to our correlation between 7.7 μm band intensity and nebular gas phase C/O ratio, namely NGC 6302, HR 4049, and the highly carbon-rich [WC 10] nucleus, CPD $-56°8032$. For the latter we have determined a ratio for C/O of $\sim$4.8 from *IUE* observations. The good correlation between the intensity ratio of the "7.7" μm feature relative to the far-infrared dust continuum and nebular C/O also supports a carbonaceous carrier for these emission features.

Subject headings: infrared: spectra — interstellar: molecules — nebulae: H II regions — nebulae: abundances — nebulae: planetary — nebulae: reflection

I. INTRODUCTION

In a previous paper (Cohen *et al.* 1986, hereafter Paper I) we presented airborne 5–8 μm spectra of objects known to exhibit the infrared emission features at 3.3, 8.7, and 11.3 μm. This study showed that (1) these bands constitute a generic spectrum of features, the most intense peaks of which are invisible from the ground (those at 6.2 and 7.7 μm); (2) although all spectra are similar, spectral variations do exist; (3) the stronger features are often accompanied by weaker ones at 5.6 and 6.9 μm (at least in some reflection nebulae); and (4) the intensity of these emission bands is tightly correlated with the gas phase C/O ratio in planetary nebulae. These bands have been attributed to fluorescent vibrational transitions in polycyclic aromatic hydrocarbon molecules (PAHs) (Leger and Puget 1984; Allamandola, Tielens, and Barker 1985), a relationship supported by the obvious link between the bands and carbon abundance (Barlow 1983; Paper I). The tight correlation between the 6.2 and 7.7 μm features supports this picture, since both originate in C=C skeletal modes in PAH molecules.

With the advent of the *IRAS Low-Resolution Spectral Atlas* (1986; hereafter LRS) it is now readily possible to select "PAH emission sources" for airborne study. Our primary source selection criterion was the presence in the *IRAS* LRS data of a rapid increase in flux density at the shortest LRS wavelengths, indicating the presence of the "7.7 μm" band, accompanied by an 11.3 μm emission band. In many objects, this pair of features occurs in combination with a plateau of emission between the 11.3 μm infrared band and $\sim$13.0 μm, including the new feature at 12.7 μm (Cohen, Tielens, and Allamandola 1985; hereafter CTA). These features, and the plateau, are generally attributed to CH out-of-plane bending vibrations of PAHs and are indicative of the molecular structures of the emitting species (CTA; Tielens *et al.* 1987). Although most spaceborne LRS spectra show evidence for both the 12.7 μm band and the plateau, poor atmospheric transmission beyond

[1] The *Infrared Astronomical Satellite* was developed and operated by the US National Aeronautics and Space Administration (NASA), the Netherlands Agency for Aerospace Programs (NIVR), and the UK Science and Engineering Research Council (SERC).

13 μm has hampered the recognition of this plateau in ground-based spectra. Recently, however, ground-based observations have confirmed the existence of the 12.7 μm peak in the plateau (Witteborn *et al.* 1988; Roche, Aitken, and Smith 1988).

Likewise, near-infrared (3–4 μm) spectra (de Muizon, d'Hendecourt, and Geballe 1987; de Muizon *et al.* 1986) have highlighted the importance of an emission plateau longward of the 3.3 μm feature, containing several minor features (e.g., at 3.40 and 3.51 μm). The relative strengths of these minor features and of the plateau vary from source to source as well as spatially within a source (Geballe *et al.* 1985, 1988; Tokunaga *et al.* 1988). These features have been attributed to "hot" bands (i.e., $v = 2 \rightarrow 1$, $3 \rightarrow 2$) of the CH stretching vibration, and overtones and combination bands of lower lying C–C stretching vibrations (e.g., the 6.2 and 7.7 μm bands; Barker, Allamandola, and Tielens 1987). Alternatively, these weaker bands may be due to CH stretching vibrations of functional groups (e.g., $-CH_2$, $-CH_3$ groups) replacing a hydrogen atom at the periphery of the aromatic carbon network of the PAHs (Duley and Williams 1981; de Muizon *et al.* 1986). In either case, the observed variations are ascribed to the photochemical evolution of small PAHs in the intense far-ultraviolet (FUV) radiation field of some sources (Geballe *et al.* 1988).

Bregman *et al.* (1988; hereafter Paper II), in a study of the Orion Bar region, have shown that the plateau between 11 and 13 μm is not spatially distributed like the sharper PAH features, whereas the 3–3.6 μm plateau follows these bands. They identify the 11–13 μm plateau with nonequilibrium emission from amorphous carbon grains. Similarly, they explain the broad 6–9 μm plateau of emission, underlying the 6.2 and "7.7" μm features and well shown by some of the spectra presented in Paper I and in the present paper, as due to clusters of PAH molecules rather to discrete, anharmonically overlapping, molecular bands from many different PAHs.

Ground-based and spaceborne observations clearly reveal that the spectrum of the infrared bands and, by inference, the nature of their carriers, vary with the physical conditions and past history of the emitting PAH family. Unfortunately, the 3–4 and 8–22 μm regions, accessible from the ground, are dominated by CH stretching and bending vibrations and give only indirect information on the structure of the carbon backbone. The strong C–C stretching vibrations occur in the 5–8 μm region, currently accessible only from NASA's Kuiper Airborne Observatory (KAO). Our previous 5–8 μm studies (Papers I and II) have already shown important spectral and spatial variations. We set out to assemble a much larger sample of airborne spectra, to compare the 5–8 μm spectral characteristics with source type and with features in other wavelength regimes. Such studies are essential for the identification of the specific molecular carriers. Although the data presented here are not sufficient for such a purpose, they do constrain the possibilities and extend the range of physical and chemical conditions in which the PAHs are found.

Our new observations were obtained during four expeditions of the KAO to the southern hemisphere primarily to pursue Comets P/Halley (1986) and Wilson (1987) and supernova SN 1987A. All objects appear in the LRS Atlas, and 10 are from CTA's sample of 20 sources with the long-wavelength plateau of emission (beyond 11.3 μm) and the 12.7 μm feature (where this is unlikely to be confused by the 12.8 μm [Ne II] line, as happens in some planetaries and H II regions). Other criteria for inclusion in our program were the existence of either a 3.3 μm feature known prior to the *IRAS* survey (e.g., for Roberts 22, an unusual OH/IR source associated with a bipolar nebula), or an 11.3 μm band with other peculiarities (e.g., in the B9.5 hypergiant, HR 4049; Lamers *et al.* 1986). A 3.3 μm emission feature is often a sharper discriminant of potential interest between 5 and 8 μm than the shape of the 11 μm region in an LRS spectrum, since the 10–20 μm LRS spectrum of cool objects is dominated by a steep rise which can entirely dwarf any 11.3 μm band. Roberts 22 (=IRAS 10197−5750) is an excellent example of this phenomenon. Almost all the sources observed have photographically nebulous counterparts.

Laboratory spectra of most PAHs show a band in the 5.1–5.3 μm range which is ~2–3 times stronger than the features in the 5.5–6 μm region (e.g., see Allamandola, Tielens, and Barker 1987). Consequently, such a feature has been predicted for astrophysical PAH sources, especially those with the minor (5.6 or 6.9 μm) bands (Allamandola 1987). While this wavelength regime is, in principle, accessible from the ground, airborne observations are better for searching at these frequencies and offer an opportunity to calibrate the relative intensity of any new band with respect to the already known PAH bands, at the same time, and through the same aperture. A recent high-resolution KAO spectrum of the planetary nebula BD +30°3639 clearly shows this new emission feature, peaking at ~5.23 μm, with a FWHM of ~0.1 μm (Allamandola *et al.* 1989; Paper IV). We shall demonstrate that this new band occurs in a wide variety of objects, offering another potential probe of carrier type.

In this paper we describe our observations (§ II); discuss the individual objects and their KAO spectra, and point out the existence of an extended plateau of emission linking the strong 6.2 and 7.7 μm features in the [WC 10] nuclei (§ III); confirm the existence of a new weak PAH band near 5.2 μm (§§ III and IV); independently confirm the correlation between the two strongest emission features (§ IV); quantitatively redetermine the intensities in the "generic spectrum" of features first proposed in Paper I, including the newly recognized 5.2 μm band (§ V); and include three more planetaries in the correlation first shown in Paper I between 7.7 μm band strength and nebular gas phase C/O ratio (§ V). Our general conclusions appear in § V.

II. THE OBSERVATIONS

Data were obtained during the periods 1986 April 8–10 (on the P/Halley expedition), 1987 April 21–24 (on the Comet Wilson/SN 1987A trip), 1987 November 10–14 and 1988 April 9–10 (SN 1987A expeditions). Table 1 presents the journal of our observations. All spectra were taken with the Faint Object Grating Spectrometer (FOGS; Witteborn and Bregman 1984) at altitudes between 11.9 and 12.5 km. During the latter three expeditions, offset guiding of optically invisible *IRAS* sources was performed by a 300 × 250 pixels CCD TV camera linked to a Commodore 64 computer implemented by one of us (D. M. R.). After 1987 April we used the Commodore and CCD camera to provide autoguiding in the KAO focal plane. Chopping of the infrared signals was at a frequency of either 14 Hz (1987 November and 1988 April) or 25 Hz (1986 April and 1987 April), with beam separations typically of 100″. Our aperture was always 22″ in diameter, and resolution ($\lambda/\Delta\lambda$) was ~50. Our spectral resolution is well-matched to the detection of variations in the 7.7 μm feature and simultaneously covers a broad wavelength region. Repeated in-flight measurements of

TABLE 1

JOURNAL OF OBSERVATIONS OF SOUTHERN IRAS SOURCES

Object	Date	Integration Time (minutes)	Standard Star	Category[a]
He 2–113	1986 Apr 8	15	α Boo	CTA
CPD –56°8032	1986 Apr 8	20	α Hya	CTA
[b]	1986 Apr 8	10	α Hya	
Roberts 22	1986 Apr 8	14	α Boo	3.3
08513–4201	1986 Apr 8	10	α Boo	CTA
	1986 Apr 10	20	α Boo	CTA
η Car	1986 Apr 10	4	α Boo	Test
VY CMa	1986 Apr 10	4	α Hya	Test
HR 4049	1987 Apr 21	10	α Sco	11.3
[b]	1987 Apr 21	12	α Sco	
He 2–77	1987 Apr 24	26	σ Lib	CTA
RCW 108	1987 Apr 24	26	α Sco	CTA
MWC 922	1987 Apr 25	20	α Sco	3.3
NGC 6302	1987 Apr 25	34	α Sco	
12389–6147	1987 Apr 25	30	α Sco	CTA
G333.6–0.2	1987 Apr 27	6	α Hya	[c]
09014–4736	1987 Nov 10	22	α CMa	CTA
05044–0325				
Peak	1987 Nov 10	30	α CMa	CTA
Star	1987 Nov 12	4	α CMa	
SW	1987 Nov 12	12	α CMa	
08485–4419	1987 Nov 12	6	α CMa	CTA
16313–4840	1988 Apr 9	26	α Hya	11.3
16396–4429	1988 Apr 9	20	α Hya	11.3

[a] CTA: source appears in the sample of 20 discussed by CTA. 3.3: source was known to show the 3.3 μm emission feature. 11.3: source was known to show the 11.3 μm emission feature in its LRS spectrum. Test: bright object observed to test our ability to remove telluric spectral features; NGC 6302 and G333.6–0.2 were observed for reasons described in the text.

[b] CPD –56°8032 and HR 4049 were observed in a second grating setting between 7.7 and 10.3 μm.

[c] G333.6–0.2 was observed twice between 5 and 8 μm with one-half channel shift between the two wavelength scales to provide an accurate wavelength calibration for this flight series.

an internal blackbody source through a polystyrene filter provided wavelength calibration. Flux calibration was achieved by observations of standard stars (α Boo, α Hya, σ Lib, α CMa), assumed to be featureless from 5 to 11 μm at our resolution. This assumption was vindicated by cross-calibration of hot and cool standards. In addition, we used α Sco for calibration due both to its infrared brightness and its location for flight planning purposes. This star shows a broad, smooth, silicate emission feature, but it is well-behaved between 5 and 8 μm and its flux densities at the longer wavelengths are represented by Merrill and Stein's (1976) filterwheel spectrum which provides an adequate calibration for our needs. To check further the behavior of α Sco between 5 and 8 μm, we cross-calibrated it against α Hya and found it to be smooth and well-described by a 3350 K blackbody.

Telluric features were removed by use of spectra of these same standards taken near cruising altitudes. The spectra of η Car and VY CMa (Fig. 1), reduced with respect to α Boo and α Hya, demonstrate the good atmospheric correction and flux calibration possible. Their high signal-to-noise enables us (incidentally) to preclude weak absorption or emission features in both sources. (Note that "dead" detectors have been removed from any spectra shown in this paper. These were usually channels 5 and 23 although, in 1986, detectors 3 and 23 were the only nonfunctioning detectors.)

During the course of these southern expeditions we have steadily improved the performance of the FOGS detectors and electronics. We have greatly enhanced the efficiency of the data acquisition software and of the general operation of the FOGS by utilizing a compiled version of the original BASIC code and by minimizing the need for keyboard interaction with the Apple computer by using the autoguider. In our earlier expeditions, we achieved 1 σ noise figures of 5E-18 W cm^{-2} μm^{-1} in 30 minutes of integration. By late 1987 and early 1988 this figure had improved to ~2E-18 W cm^{-2} μm^{-1} in 30 minutes.

We present our spectra as linear plots of F_λ versus λ, with error bars representing the root sum square combinations of the photometric statistics for each detector in the array and photometric errors in the standard star spectra. Also plotted, as dashed lines, are continua, spline-interpolated between ground-based spectrophotometry or photometry, shortward of 5 μm and longward of 8 μm, or by combining short-wavelength ground-based data with LRS spectrophotometry at ~10.0 to 10.5 μm (avoiding the known PAH emission features). For point sources we used both the literature and the LRS spectra directly. Otherwise we have sought published information with apertures as close as possible to our own, we have normalized the LRS spectra to the KAO data in their region of overlap (~7.7–8.1 μm) before using LRS data near 10 μm and have rescaled 3.3 μm data to our 22″ beam, assuming uniformity of surface brightness across this aperture.

The integrated band strengths above the interpolated continua, for the strong 6.2 and 7.7 μm features and the weaker 5.2, 5.6, and 6.9 μm bands, appear in Table 2. This table also gives published data, with references, for the strength of the 3.3 μm features.

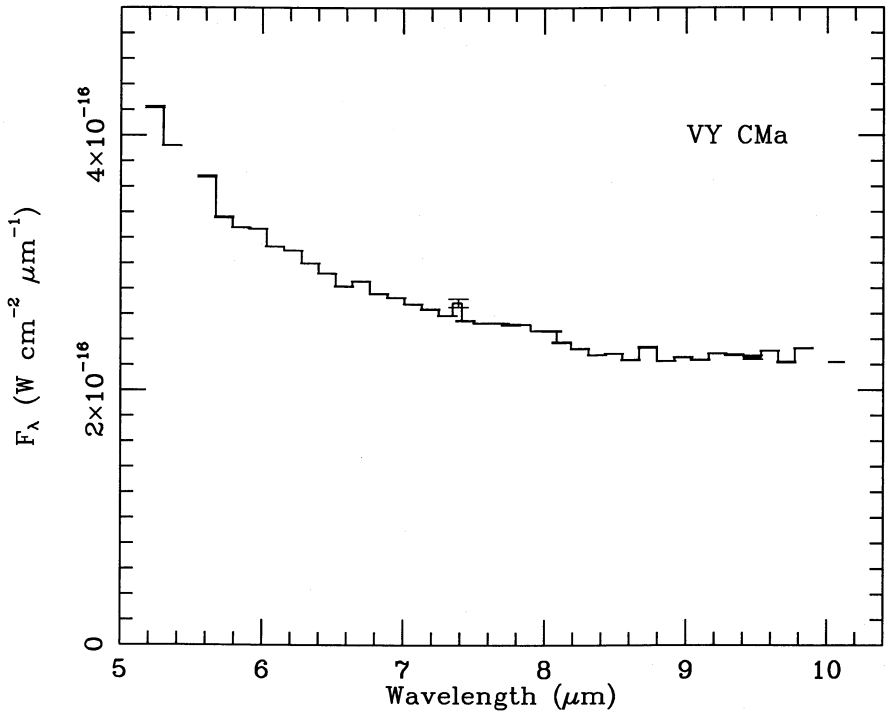

FIG. 1*a*

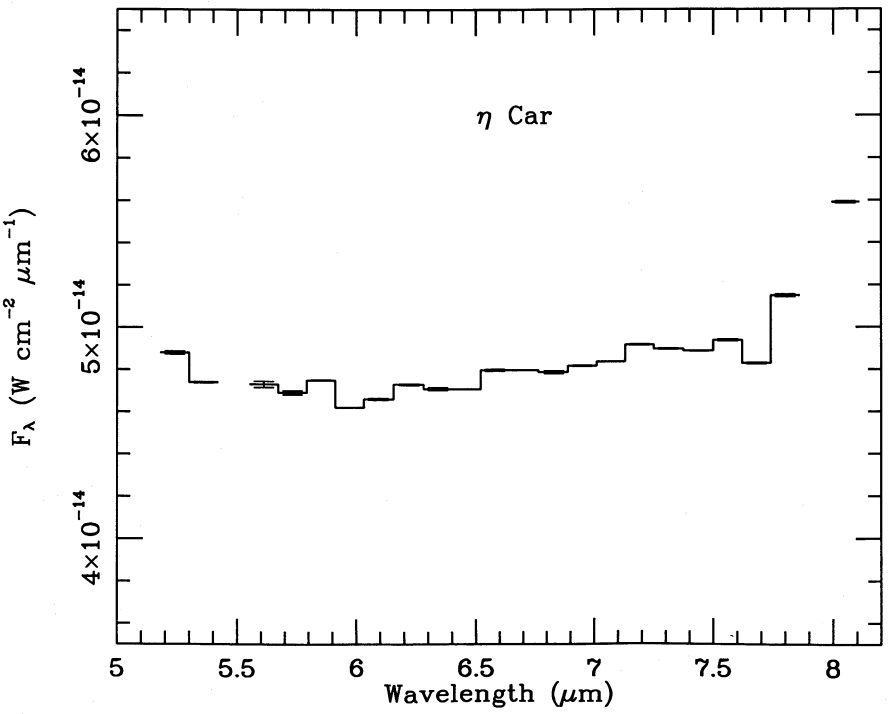

FIG. 1*b*

FIG. 1.—(*a*) The FOGS spectrum of VY CMa obtained from the KAO. Ordinate is F_λ in W cm^{-2} μm^{-1}; abscissa is λ in μm. (*b*) As (*a*), for η Car; the rise beyond 7.8 μm is real and represents the onset of the known silicate emission feature (see Aitken and Jones 1975).

TABLE 2

INTEGRATED BAND STRENGTHS (units are 10^{17} W cm^{-2})

SOURCE	λ(μm) 3.3	5.2	5.6	6.2	6.9	7.7	NEBULAR TYPE[a]	3.3 μm NOTES
CPD −56°8032	0.89	0.48	<0.06	9.8	0.45	37.0	PN	b, c
He 2–113	0.55	0.17	<0.04	6.4	0.29	23.3	PN	b, c
Roberts 22	0.37	0.35	...	6.8	<0.04	13.0	PN	b, c
He 2–77	0.39	0.09	<0.05	1.3	0.10:	2.5	PN	d
RCW 108	0.74	0.18	0.07	3.5	Ar II	5.2	H II	c, d
MWC 922	0.65	0.67	...	7.9	0.20	24.9	PN[e]	f
NGC 6302	...	...	Mg V	0.37	Ar II	2.9:	PN	
G333.6−0.2	...	0.46	0.07	4.8	Ar II	9.6	H II	
HR 4049	<0.13	1.2:	...	1.8	...	12.0	PN	
05044−0325								
Peak	0.06	<0.14	...	0.60	...	1.1	RN	d
Star	...	...	...	0.21	...	0.31	RN	
SW	...	...	...	0.55	...	0.83	RN	
08485−4419	...	0.09	<0.1:	1.5	<0.2	2.3	H II	
08513−4201	0.05:	0.04:	0.02:	1.7	<0.1	4.4	RN	c
09014−4736	<0.07	<0.03	<0.08	0.57	<0.06	1.3	RN	c
12389−6147	0.35	1.1	0.33	3.4	<0.18	4.1	H II	d
16313−4840	...	...	...	0.60	0.30	1.1	H II	
16396−4429	...	...	...	1.5	0.12	2.4	H II	

[a] Types are PN, planetary or protoplanetary nebula; RN, reflection nebulae; H II, H II regions.
[b] 3.3 μm intensity from Allen *et al.* 1982 and large-scale calibrated plots of original spectra from Allen 1987.
[c] 3.3 μm intensity from P. McGregor; 11″ square aperture, ANU 2.3 m telescope.
[d] 3.3 μm intensity from de Muizon, d'Hendecourt, and Geballe 1987*a* with apertures: IRAS 05044−0325, 12.″4; 12389−6147, 15″; He 2–77, 15″; and RCW 108, 12.″4.
[e] We assign MWC 922 to the category of PN since it may represent a compact emission-line object akin to PN.
[f] 3.3 μm intensity from M. Cohen and D. A. Allen (see § III, on MWC 922).

III. INDIVIDUAL SOURCES

In what follows we describe the individual sources that we have observed and present their KAO spectra. When examining these spectra, the reader should watch for several characteristics that occur in some or all sources: a redshading, or asymmetry, of the 6.2 μm band, or a pedestal beneath this feature; emission infilling the region between the 6.2 and 7.7 μm bands but substantially above the interpolated continua; potential variations in the actual peak of the "7.7" μm peak; a 5.2 μm band; and a 6.9 μm band.

a) The [WC 10] Planetary Nebula Nuclei, CPD −56°8032 (=IRAS 17047−5650) and He 2–113 (=IRAS 14562−5406)

The rare, very low excitation [WC 10] nuclei have among the coolest stellar temperatures (as low as 22,000 K; Goodrich and Dahari 1985) and lowest velocity winds (<300 km s^{-1}) of the sequence of carbon Wolf-Rayet nuclei in planetary nebulae (see Webster and Glass 1974; cf. the [WC 11] nucleus of IRAS 21282+5050; Cohen and Jones 1987). Figures 2 and 3 present our airborne spectra. Both CPD −56°8032 and He 2–113 are infrared point sources, and the continua were directly interpolated between ground-based infrared data (broad-band photometry at 3.5 and 4.7 μm from Cohen 1975) and narrow-band spectrophotometry at 9.0 μm from Aitken *et al.* (1980). Indeed, for CPD −56°8032, Aitken *et al.*'s (1980) 9.0 μm flux density level (with a 3.″6 beam) agrees exactly with ours in a 22″ beam. Similarly, good agreement is obtained with the *IRAS* LRS spectra, especially near the 7.9 μm peak, for both [WC 10] stars. Therefore, we are confident of the appropriateness of our interpolated continua.

Both objects show a potentially new feature at 5.2 μm. Several sources discussed below clearly show a channel significantly elevated approximately at this latter wavelength (often the first channel of our spectrum). The low-resolution spectra detailed in the present paper are inadequate to define the extent of this new feature. However, we note the feature at ~5.2 μm discovered in BD +30°3639 (see § I) with FWHM very close to the spectral width of a single FOGS detector. Generally, the first detector is centered at 5.25 μm in these observations, and the flux in the 5.2 μm feature derived from this detector should be a reasonable approximation to the real band strength. However, small variations in the center wavelength of this channel may introduce relatively large uncertainties in the derived flux of the feature.

In general, *all* our KAO spectra show higher levels of emission at ~6.6 μm than at 5.8 μm, but usually the 6.6 μm level is close to the splined continuum. In these [WC 10] spectra, however, we see an obvious plateau of low-level but apparently continuous emission, lying substantially above the interpolated continuum, and filling in the entire spectral region between the strong 6.2 and "7.7" μm bands. Such a plateau is also shown by spectra of the Orion Bar (Paper II) and of reflection nebulae (NGC 2023 and 7023; Sellgren *et al.* 1985), and may be present weakly in the spectra of the planetaries M 1-11 and BD +30°3639 (Paper I), but not as prominently as in the [WC 10] nuclei. Since we obtained consecutive KAO spectra of CPD −56°8032 on a single KAO flight, there is no doubt as to the reality of this plateau between 6.2 and 7.9 μm: the continuum level in this source decreases longward of the 8.7 μm PAH feature and clearly indicates the unusual height of the spectrum between the dominant emission bands.

b) Roberts 22 (=IRAS 10197−5750)

Each lobe of this tiny (3″) optical bipolar nebula reflects the spectrum of an A2 supergiant (Allen, Hyland, and Caswell 1980). Known originally as an OH source (Manchester, Goss,

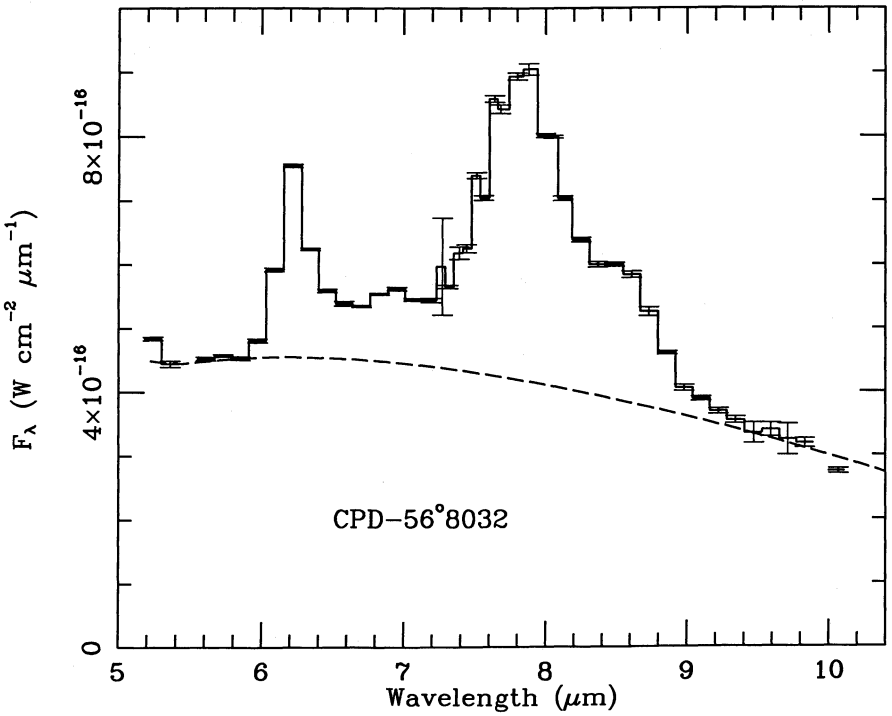

FIG. 2.—As Fig. 1 for the [WC 10] planetary nucleus, CPD −56°8032. Interpolated continuum is as described in the text.

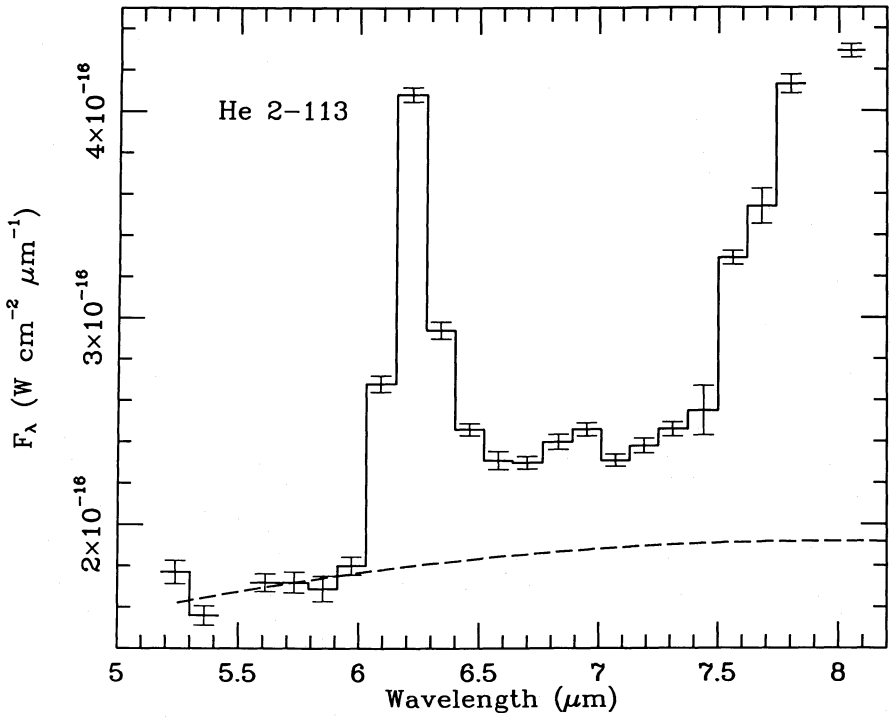

FIG. 3.—As Fig. 2, for the [WC 10] planetary nucleus, He 2–113

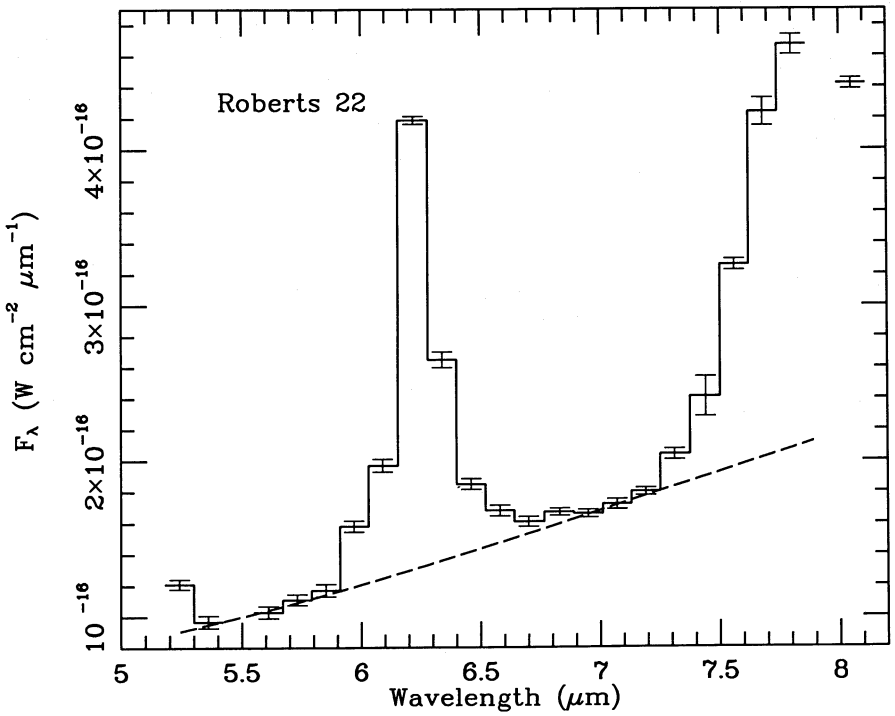

FIG. 4.—As Fig. 2, for the protoplanetary nebula, Roberts 22

and Robinson 1969), the infrared emission was first localized by Frogel and Persson (1975). Although the redshifted OH component is weak, Roberts 22 has the twin-peaked OH emission spectrum of a typical, cool red giant, OH/IR source. Allen, Hyland, and Caswell suggest, by comparison with several other bipolar nebulae, that the source is a protoplanetary nebula, evolving from the tip of the asymptotic giant branch to the Harman-Seaton sequence of planetary nebulae. Allen *et al.* (1982) reported the existence of a 3.3 μm emission feature in Roberts 22's near-infrared spectrum although there is no obvious 11.3 μm feature in the LRS data. Figure 4 shows our spectrum with an interpolated continuum based on the ground-based photometry of Frogel and Persson (1975) and these authors' determination that the infrared emission at 2 and 10 μm was pointlike. The flux density in the KAO spectrum near 8.0 μm is in excellent agreement with that determined from the LRS spectrum. This, combined with the broad agreement between McGregor's more recent 3 μm spectrum and that of Allen *et al.* (1982) through a different aperture, confirms our assumption of a point infrared source. The 6.2 μm band appears on a pedestal (see Paper I).

c) He 2–77 (=IRAS 12063−6259)

This roughly triangular nebula was observed by Cohen and Barlow (1980) in relatively narrow bands during their photometric survey of planetary nebulae. These authors felt that the object might actually be a reddened H II region on the basis of its large radio flux and its Balmer decrement and cautioned that the minimum near 9.6 μm might be due to either a silicate absorption feature or to flanking (molecular) emission features. The LRS spectrum shows the 11.3 μm feature, as well as high-excitation atomic emission lines. From the existence in the KAO data of the 6.2 and 7.7 μm bands (Fig. 5) one can readily see that the LRS spectrum should be interpreted as PAH features flanking a minimum near 10 μm and not as an otherwise featureless continuum suffering extinction by silicates. Indeed, de Muizon, Preite Martinez, and Heydari-Malayeri (1987) have reclassified He 2–77 as a planetary.

The "7.7" μm peak flux density in Figure 5 is only $\sim$0.33 of the shortest wavelength flux density indicated by the LRS Atlas, indicating the large spatial extent of the infrared emission. Consequently, the splined continuum was interpolated between Allen's (1973*a*) broad-band 2.2 μm measurement and the proportionately scaled down LRS datum at 10.5 μm. This is justified also by the cross-reference for He 2–77 in the *IRAS Point Source Catalog*, version 2 (*IRAS* 1985; hereafter PSC2) to a source, X1206−629, in the *IRAS Small Scale Structure Catalog* (IRAS 1986; hereafter SSSC), whose flux density at 12 μm exceeds that given in PSC2 by a factor of 1.6, probably due to spatially extended emission in the 7.7, 8.7, and 11.3 μm features which dominate the *IRAS* 12 μm bandpass.

d) RCW 108 (=IRAS 16362−4845)

This object appears to be heavily obscured, although it is closely flanked, to east and west, by faint optical nebulosities apparently at the core of an extended H II region. The *IRAS* source corresponds to the source discussed by Frogel and Persson (1974), who provided multiaperture photometry at several wavelengths. This facilitates the interpolation of a suitable continuum between 3.5 and 10 μm as a lower envelope to our KAO spectrum (Fig. 6). The splined continuum is based on interpolating Frogel and Persson's K and L points to our 22″ aperture, and using the LRS flux density at 10.5 μm scaled down by the ratio of LRS to KAO spectra near the 7.7 μm peak. The conspicuous feature near 7.0 μm is likely to be due to the [Ar II] line at 6.98 μm, often seen in H II regions, rather than to the 6.9 μm PAH band.

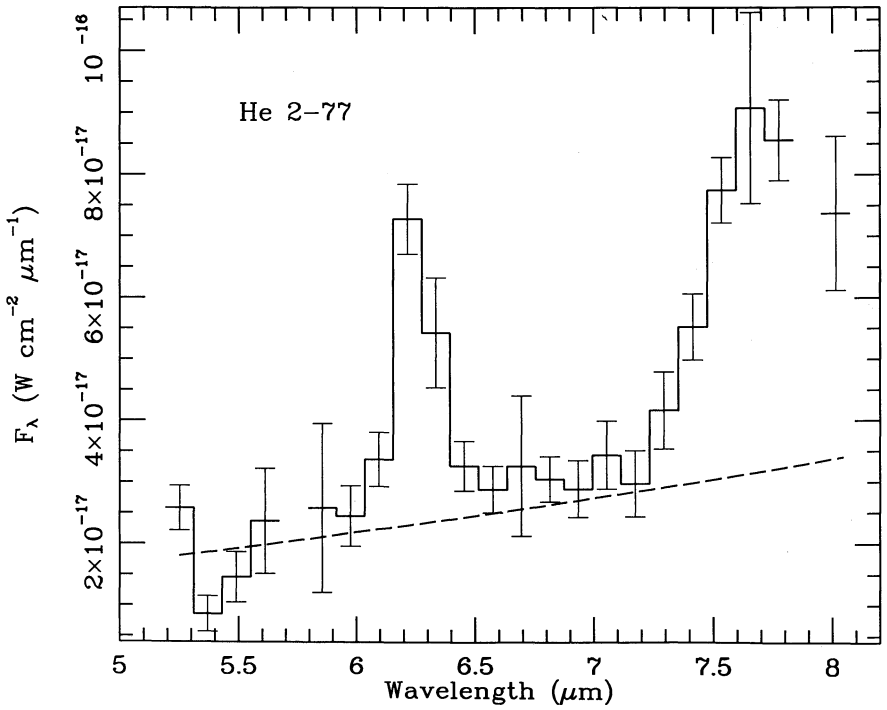

FIG. 5.—As Fig. 2, for the H II region, He 2–77

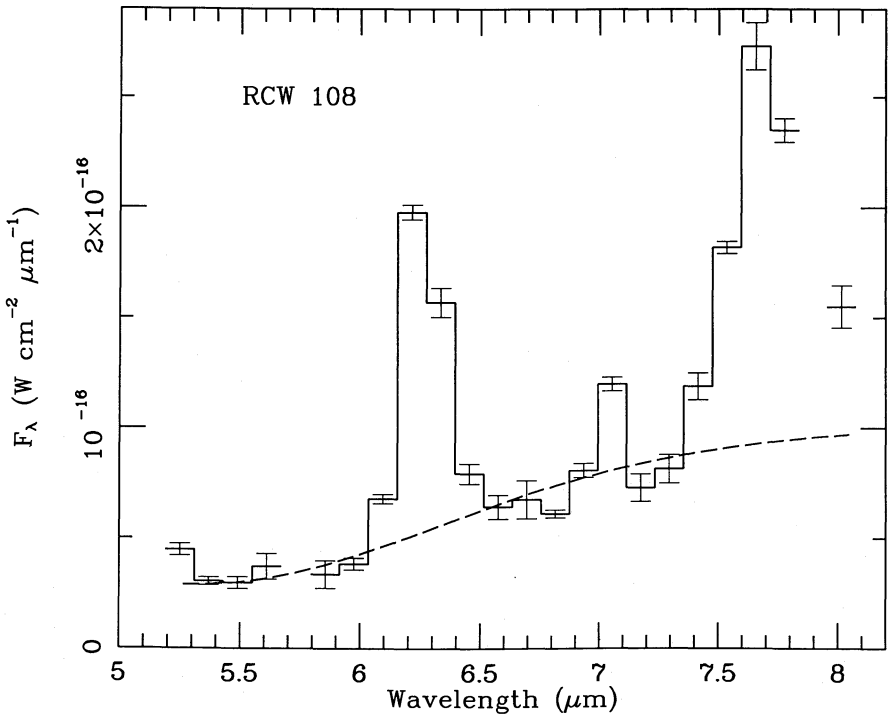

FIG. 6.—As Fig. 2, for the H II region, RCW 108

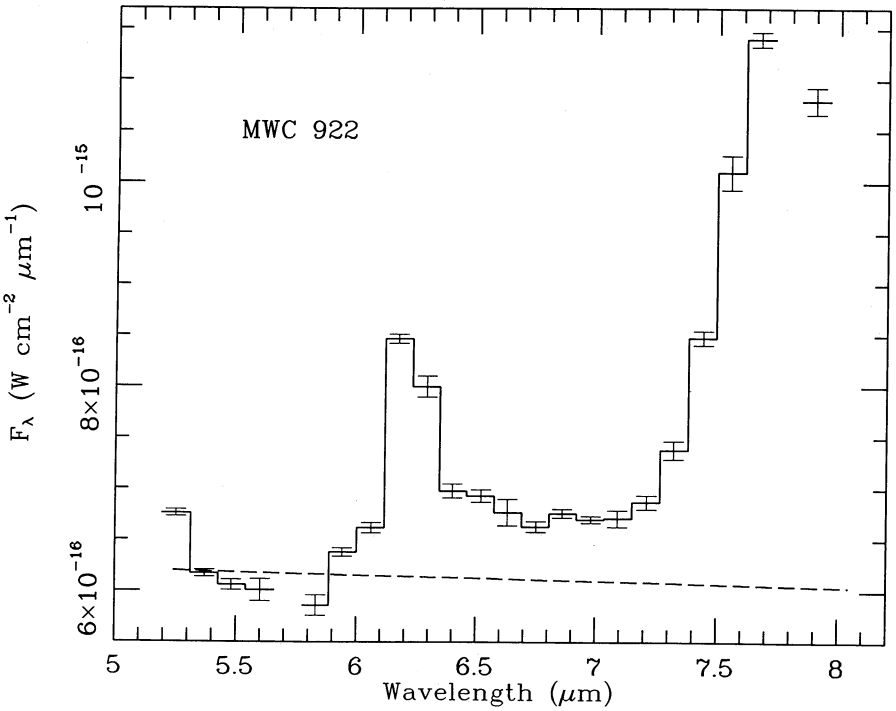

FIG. 7.—As Fig. 2, for the emission-line star, MWC 922

e) MWC 922 (=IRAS 18184−1302)

In spite of its LRS characterization as an object with the 11.3 μm emission feature, the LRS spectrum of this heavily reddened emission-line star does not unequivocally suggest the presence of an 11.3 μm band. However, an unpublished 2–4 μm spectrum with 1.5% resolution taken by M. Cohen and D. Allen in 1973 September, with the Minnesota–San Diego Mount Lemmon 1.5 m telescope, clearly indicates a 3.3 μm feature. The continuum was set by linear interpolation between the 1973 Mount Lemmon spectrum [F_λ(4.0 μm) = 5.1E-16 W cm^{-2} μm^{-1} in a 17″ beam], ground-based photometry at 5.0 μm, and the LRS flux density at 10.5 μm. There appears to be no obvious aperture dependence of peak flux density at 7.7 μm, comparing Figure 7 with the LRS shortest wavelength point. The 6.2 μm feature seems somewhat red-shaded and perched on a pedestal. MWC 922 shows enhanced emission between the 6.2 and 7.7 μm bands similar to that in the [WC 10] nuclei (Figs. 2, 3). Optically, MWC 922 shows no kinship with the carbon-dominated spectra of the WC stars but rather has a rich [Fe II] and [Fe III] emission-line spectrum (Allen 1973*b*).

f) NGC 6302 (=IRAS 17103−3702)

This high-excitation planetary nebula has a rich and obvious emission-line LRS spectrum dominated by lines of neon (e.g., Pottasch *et al.* 1985). We felt it worthwhile to observe from the KAO for several reasons. (1) NGC 6302 has an apparently very low carbon abundance (C/O ~ 0.2: Aller *et al.* 1981; Barral *et al.* 1982; but see Roche and Aitken 1986, who caution it may be essential to include very high ionization states of C and O in this nebula) which would complement the set of abundance values represented in our correlation between "7.7" μm band strength and nebular C/O (Paper I). (2) The LRS Atlas and the 8–13 μm spectrum by Roche and Aitken (1986) indicate a very weak but definite 11.3 μm emission feature. (3) An OH maser is associated with the nebula (Payne, Phillips, and Terzian 1988), also suggestive of a more oxygen-rich chemistry. (4) Pottasch *et al.* (1985, 1986) have stressed the importance of airborne data to validate their interpretation of the rapid increase at the shortest LRS wavelengths (often indicative of the long-wavelength flank of the PAH band at 7.7 μm) in NGC 6302 as due to an intense line of [Ne VI] at 7.65 μm. Roche and Aitken (1986) support this line identification, although their evidence rests on the least reliable shortest wavelength ground-based points in the 8–13 μm window.

The continuum was splined from ground-based data at 2.2 and the LRS flux density at 10.5 μm. Although there exist ground-based multiaperture observations at 3.5 and 10 μm (e.g., Danziger, Frogel, and Persson 1973), we felt it better not to use these because of the danger of contamination by line or band emission (e.g., of the 10 μm broad-band data due to [Ar III] and [S IV]). Since our KAO spectrum does not show lower flux densities than those implied by the LRS, we feel the 5–8 μm source in this complex, "polypolar" nebular (see Barral *et al.* 1982) is essentially pointlike to our 22″ beam. This conclusion is supported by Lester and Dinerstein (1984), who mapped NGC 6302 at 2.2 and 10 μm and found a disklike distribution of infrared emission on the order of 20″ in extent.

We clearly see a powerful line which peaks in our 7.67 μm channel (Fig. 8) which, we suggest, confirms the identification of [Ne VI] in this nebula. However, our spectrum also shows a 5 σ elevation above the continuum even longward of this line. It is, therefore, likely that this planetary also has PAH emission, consistent with the presence of the 8.7 and 11.3 μm features (Roche and Aitken 1986). The short-wavelength emission at 5.6 μm is identified with [Mg V], as seen in NGC 7027 (Bregman *et al.* 1983). The strength of [Mg V] is ~1E-17 W cm^{-2}. The peak near 7.0 μm is more likely to be the 6.98 μm

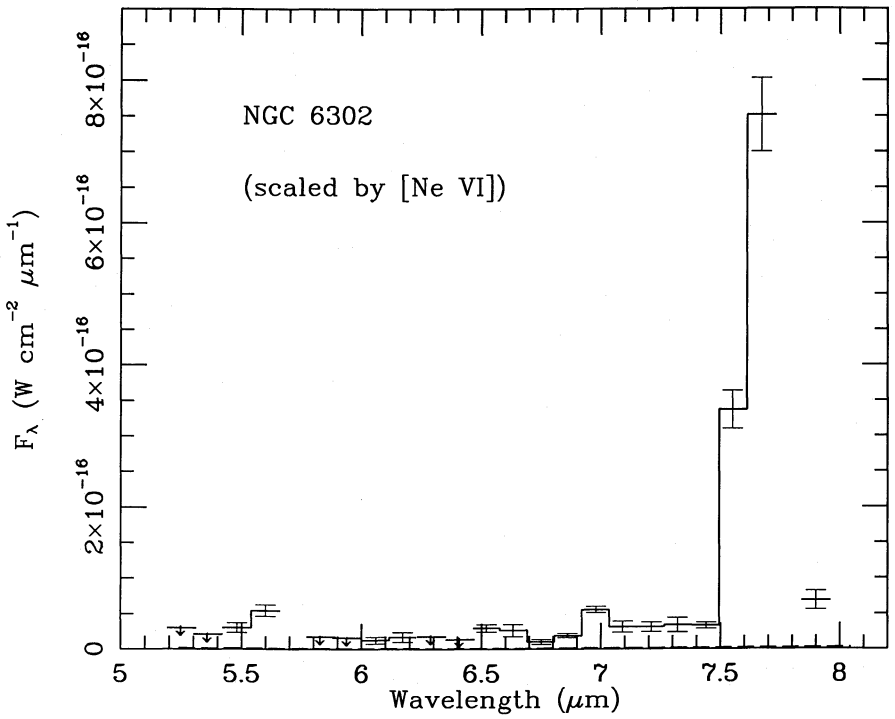

FIG. 8*a*

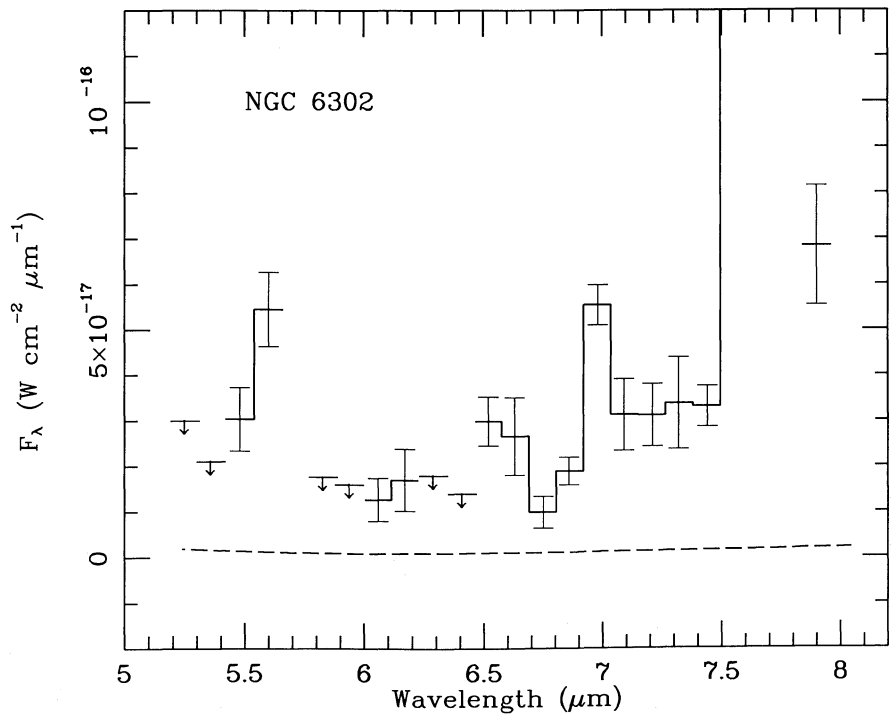

FIG. 8*b*

FIG. 8.—(*a*) As Fig. 2, for the planetary nebula, NGC 6302, showing the powerful [Ne VI] emission line. (*b*) NGC 6302 scaled to show the weaker features in the spectrum. In this and subsequent plots, 3 σ upper limits are shown in the absence of any detections in specific channels. Note the 5 σ high channel $\sim$7.9 μm (see text).

[Ar II] line than the usually weak PAH feature at 6.9 μm (Paper I).

Our flux density at the peak of the [Ne VI] line is approximately twice that implied at the line peak in the LRS spectrum as represented by Pottasch *et al.* (1986). We have rechecked our observing log, have cross-calibrated NGC 6302 against other sources in this paper whose LRS spectra compare well with ground-based observations, and have used different standard stars for fluxing our data. We can find no error in our calibration. However, the extremely rapid increase toward shorter wavelengths in the [Ne VI] line and the abrupt cut-on in LRS response make the flux calibration of the LRS suspect at its two shortest wavelengths.

Recently, Ashley and Hyland (1988) have predicted that NGC 6302 should show a [Si VII] line at 6.50 μm on the basis of their discovery of other highly ionized silicon lines, [Si VI] at 1.96 and [Si VII] at 2.48 μm. We detect a broad feature in emission between 6.45 and 6.65 μm, the long-wavelength portion of which we can plausibly attribute to the 6.64 μm [Ni II] line first observed in NGC 7027 (Bregman *et al.* 1983). [Ni II] probably contributes ~6.5E-18 W cm^{-2} to this broad feature in NGC 6302. We feel that the short-wavelength component could well be due to the predicted [Si VII] line, although our estimated imtensity (~3E-18 W cm^{-2}) is ~10 times that predicted by Ashley and Hyland (1988). However, these authors note that considerable uncertainty may lie in their inferred distribution of silicon ions among these highly excited states, which would seriously affect any predictions of line intensities.

g) G333.6−0.2 (=IRAS 16183−4958)

Persson, Frogel, and Aaronson (1976) provided narrow-band data at 9.8 μm of this powerful H II region through two different apertures, and Aitken and Jones (1974) a detailed spectrum between 8 and 13 μm in a 12″ aperture. We splined a continuum appropriate to our 22″ aperture between broad-band data at 3.5 and 4.8 μm, and Aitken's and Jones's data at 9.8 μm (this was judged to be more secure than attempting to scale down LRS data to our aperture for such a greatly extended source).

Figure 9 presents our consecutive 5–8 μm spectra, with the grating position shifted by 0.5 detectors between spectra. This provided more precise wavelength calibration for SN 1987A through the observed location of the [Ar II] line at 6.98 μm. Figure 9 interleaves the two separately flux-calibrated spectra (the smaller horizontal bars represent this interleaving of data and signify twice the resolution of our other spectra since the FOGS normally undersamples the spectrum of a point source by a factor of 3 and that of an extended source by a factor of 2).

The 6.2 μm feature seems red-shaded. Because of the rapidly increasing continuum, the peak of the "7.7" μm emission feature is difficult to determine. There appear to be two separate peaks longward of Pfα at 7.46 μm: one at 7.65 μm, the second at ~7.8 μm. We note that observations of NGC 7027 at high spectral resolution (Bregman *et al.* 1987), 3 times the resolution in the present paper, also reveal a splitting of the "7.7" μm feature into two peaks close to the same wavelengths as shown by G333.6−0.2.

h) HR 4049 (=IRAS 10158−2844)

Lamers *et al.* (1986) discussed the energy distribution of this bright star in terms of either a runaway late-B hypergiant or a less massive protoplanetary nebula. Lambert, Hinkle, and Luck (1988) published an abundance analysis of this star, concluding that it is a highly evolved, metal-poor Population II star, apparently a protoplanetary nebula caught between the tip of the AGB and the top of the cooling track for white

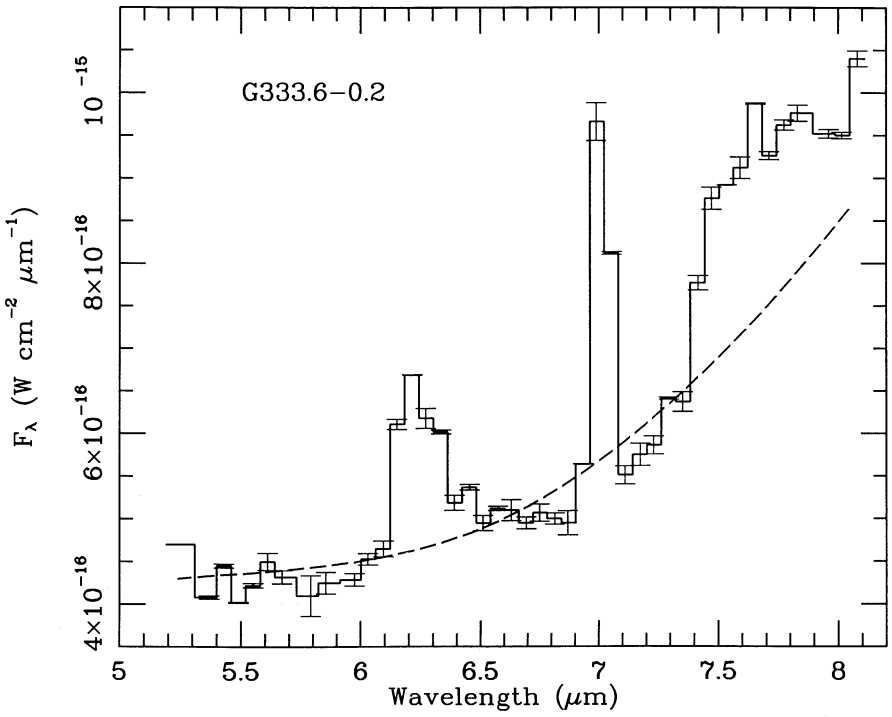

FIG. 9.—As Fig. 2, for the H II region, G333.6−0.2. Note that higher resolution data are available for much of this spectrum.

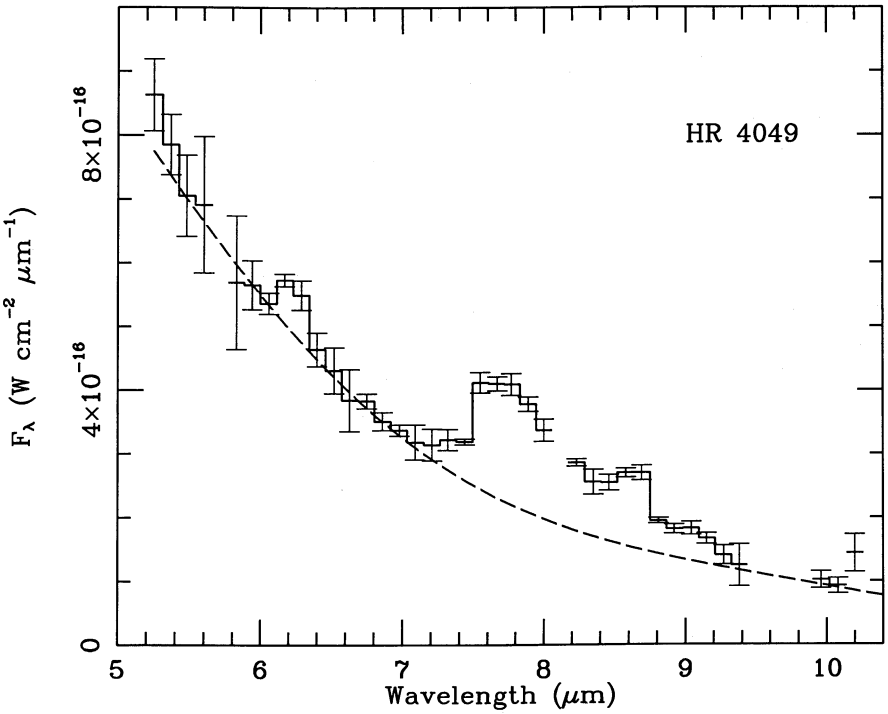

FIG. 10.—As Fig. 2, for the protoplanetary nebula, HR 4049

dwarfs. The star may well be carbon-rich: Lambert *et al.* derive a probable, but uncertain, estimate for C/O of ~2. The LRS spectrum clearly shows an 11.3 μm feature, and it may have a generally elevated, although weak, plateau from 11 to 13 μm. Figure 10 presents our 5–10.5 μm spectrum, taken in two consecutive sections (5.25–7.90 and 7.66–10.30 μm) by rotating the FOGS grating. The continuum was actually set by splining between the 3.8 μm point of Lamers *et al.* and the LRS flux density at 10.0 μm, but provides an excellent fit to the KAO spectrum. We clearly detect peaks at 6.2, "7.7", and 8.6 μm, above this continuum. HR 4049's 7.7 μm emitting region appears to be pointlike on the scale of our beam from comparison of the KAO and LRS flux densities near 7.7 μm.

HR 4049's infrared spectrum strongly resembles those of the Population I WC 8–9 Wolf-Rayet stars, Ve 2-45 and GL 2104, which Cohen and Tielens (1989) attribute to amorphous carbon material.

i) IRAS 05044−0325

This *IRAS* source is associated in the PSC2 with the SSSC object X0504−034. The ratio of SSSC to PSC2 flux densities at 12 μm (2.3) exceeds that at 25 μm (1.8). Perhaps 05044−0325 is another example of a source with widely dispersed PAH emission.

The *IRAS* source position nearly coincides with that of a star in the nebula, Cederblad 40. We observed at four positions: (*a*) at the nominal *IRAS* coordinates, 6″.5 E of this star, in the amorphous nebula (Fig. 11*a*); (*b*) at the nebulous star (Fig. 11*b*); (*c*) 22″ to the SW of the star (close to the NE boundary of an obvious patch of local obscuration; Fig. 11*c*); and (*d*) 22″ to the NE of the star (spectrum not shown). In all four positions we obtained spectra with nonzero channels near the 6.2 and "7.7" μm features. The very brief spectrum in the NE position demonstrated only the presence of the PAH peaks but yielded no quantitative data. In no position does our airborne spectrum achieve the LRS flux density at ~7.7 μm. We suggest, from both the SSSC information and our own KAO data, that Cederblad 40 is an extended reflection nebula, with spatially distributed PAH emission, and with a small H II region close to the central star. The SW spectrum supports this view since we detect essentially nothing except the 6.2 and 7.7 μm bands (Fig. 11*c*).

Our continua in these spectra are flat, equal to the LRS value at 10.0 μm for the nominal *IRAS* peak position, and zero elsewhere. From Figures 11*a* and 11*b* we can synthesize the spectrum of the star itself by subtracting the spectrum at the *IRAS* peak from that taken at the star's location, resulting in a spectrum that reveals absolutely no continuum, virtually no 7.7 μm band, but an obvious Pfα emission line, betraying an origin in a recombination zone driven by this star. (The Pfα line is also obvious in Fig. 11*b* itself.)

j) IRAS 08485−4419

This source from CTA's sample corresponds to a blank field on the SERC/ESO *J* and *R* southern sky plates. Two extremely faint objects appear on the *I* transparency, but it is unclear whether either is a counterpart to the *IRAS* source. We were able to obtain only 6 minutes of integration time on this source; consequently, the spectrum shown in Figure 12 is noisy. The emission seems spatially extended since our peak flux density at 7.7 μm is only about half of the LRS value. The splined continuum is designed to reflect the LRS level at 10.0 μm (scaled down in accordance with the ratio of the KAO and LRS values at 7.7 μm) and roughly to match our spectrum around 5.35 and 6.8 μm.

k) IRAS 08513−4201

This source was among the 20 that CTA identified as showing the new 12.7 μm emission feature on the 11–13 μm

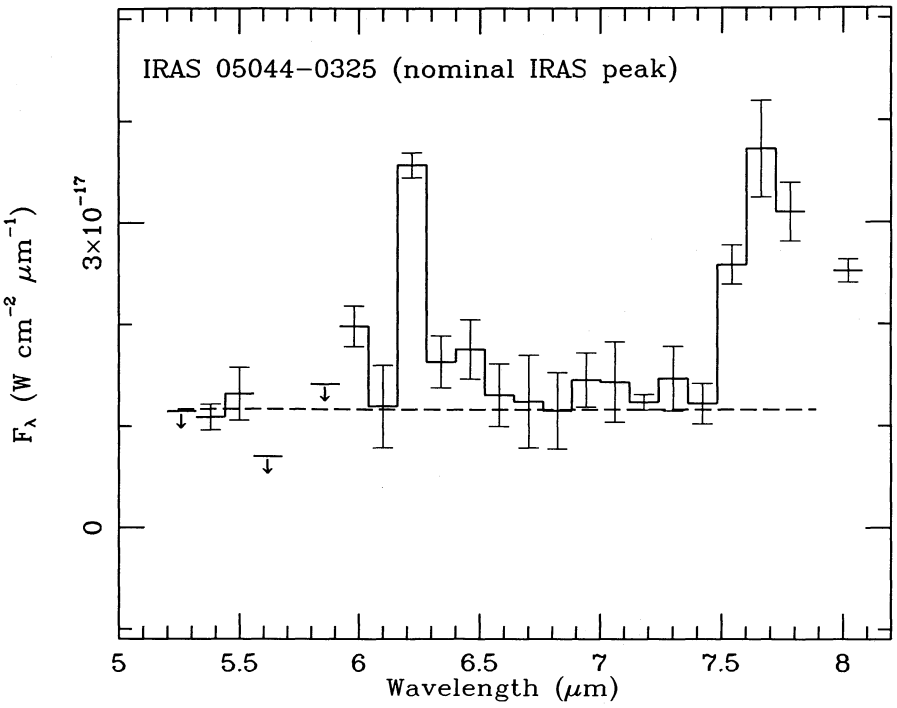

FIG. 11*a*

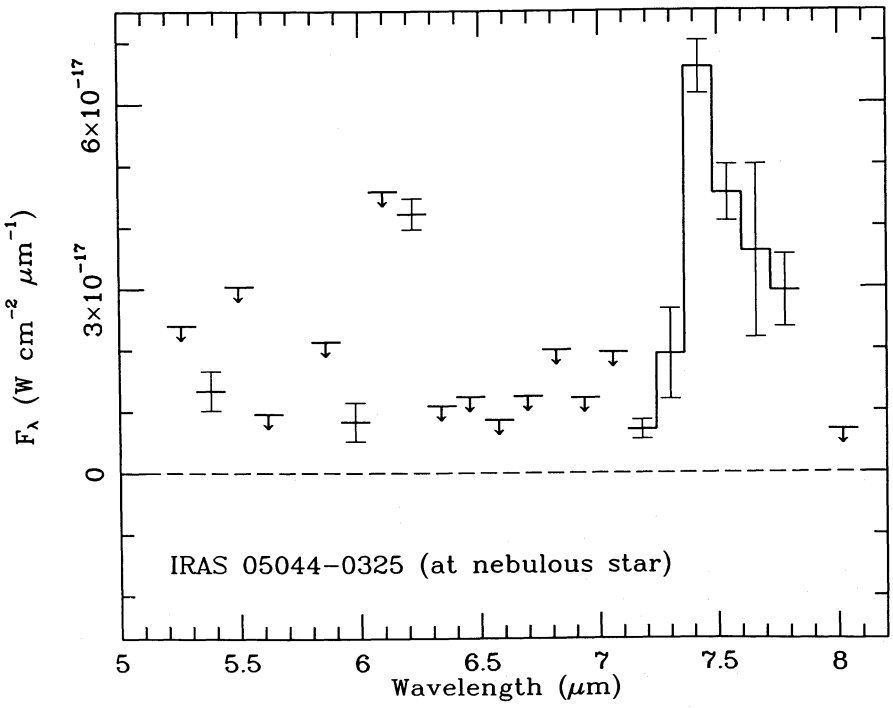

FIG. 11*b*

FIG. 11.—As Fig. 2, for the reflection nebula, IRAS 05044−0325, at (*a*) the nominal IRAS peak; (*b*) the nebulous star; (*c*) 22″ SW of the nebulous star.

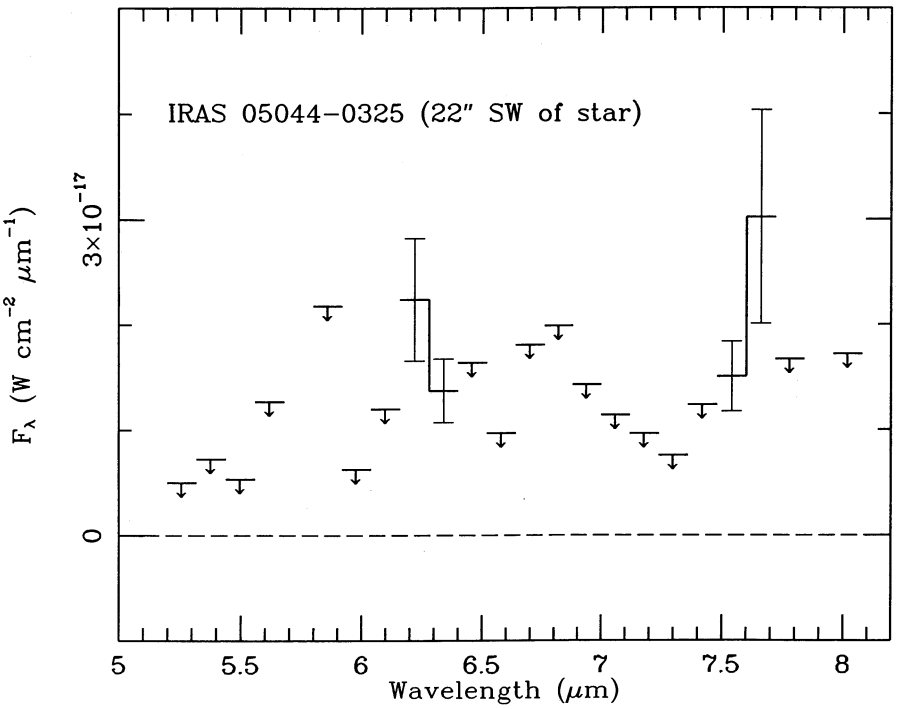

FIG. 11*c*

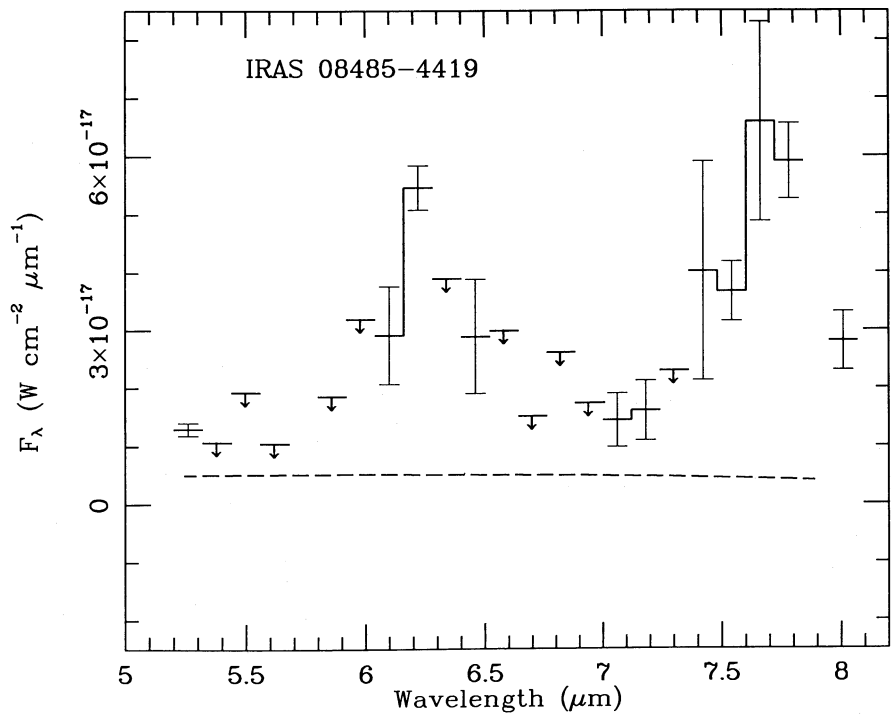

FIG. 12.—As Fig. 2, for the H II region, IRAS 08485−4419

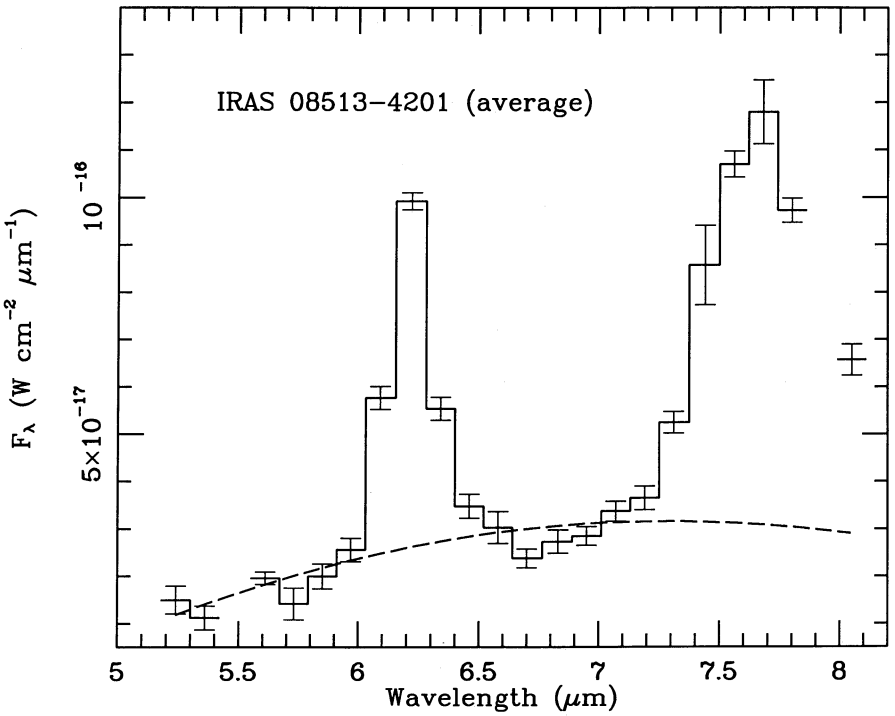

FIG. 13.—As Fig. 2, for the reflection nebula, IRAS 08513−4201; spectrum shown is the average of two essentially identical spectra

plateau. Photographically it coincides with a cometary nebula—a fan, extended essentially east to west, with an obvious brightening at the apex to the east. This bright condensation is brighter on the blue than on the red or near-infrared photographs. Immediately to its northwest the nebular rim is concave and contains a faint red star. PSC2 associates the object with one of Wesselius's unpublished list of globules, DC 263.2+01.6. The morphology and color of the nebulosity suggest that it is a reflection nebula, consistent with absence of conspicuous emission lines in star or nebula (Cohen and Wainscoat, unpublished spectra from 1988 May).

We took a series of KAO spectra on a spatial grid with 11″ spacing around the nominal peak to be sure that our long offset from the nearest guidable star did not miss the *IRAS* peak. We found only a point source. The single spectrum at our defined peak on 1986 April 10 reproduced almost exactly that found from the 1986 April 8 map. Figure 13, therefore, shows the average of these two spectra. There is excellent agreement between the flux levels in the LRS spectrum and in our airborne data at the peak of the "7.7" μm band, strengthening our conclusion that the source is pointlike in our beam. We have no ground-based photometry but the LRS data yield a flux density in the continuum at 10.0 μm of 3E-17 W cm^{-2} μm^{-1}. Consequently, we interpolated a continuum that simultaneously matches the short spectral segments near 5.3 and 6.6 μm, and agrees with the LRS flux density at 10 μm that is uncontaminated by any PAH features.

l) IRAS 09014−4736

Figure 14 presents our KAO spectrum of this very red, extremely faint nebula. It is a fan, elongated roughly east-west on the Southern Sky Survey photographs, with a very red star located at its western apex. Its infrared emission is extended, both by comparison of KAO and LRS spectra, and by virtue of its association with the object X0901−476 although the SSSC lists spatial extension only at 25 and 60 μm. Our splined continuum links the KAO segment near 5.3 μm to the LRS 10.0 μm flux density, scaled down from the KAO-to-LRS ratio at 7.7 μm.

m) IRAS 12389−6147

Another of CTA's sample, this source coincides on the SERC Southern Sky Survey *J* and *I* photographs with a red star associated, to its immediate south, with an elongated wisp of very red nebulosity, extended in P.A. = 155°. However, long integration through our focal-plane CCD TV guider on the KAO revealed neither star nor nebulosity despite our ability to see stars as faint as the *J*-plate shows. Probably the extreme redness of both star and nebula, coupled with the presence of a gold beamsplitter just ahead of our CCD TV camera, conspire to pass very few photons to the CCD.

The source is pointlike, comparing the KAO and LRS data near 7.7 μm, so we interpolated a continuum that is flat, matching the LRS level at 10.0 μm. This pointlike character seems consistent with the sharpness on the photographs of the nebula, which resembles one lobe of a faint bipolar nebulosity. Such a nebula is usually dominated by the emission of its central star in the infrared.

The spectrum shows a 6.2 μm feature perched on a pedestal. Figure 15 shows a rapid rise to short wavelengths, but we have no near-infrared photometry to define a suitable continuum near 5 μm. If this rise is due solely to another "5.2 μm" feature, then it is unusually bright. This assumption was made to provide the estimated 5.2 μm band strength in Table 2 for this source.

n) IRAS 16313−4840

On the Southern Sky Survey transparencies, this *IRAS* source coincides with a small (~3″), faint, red nebulous patch

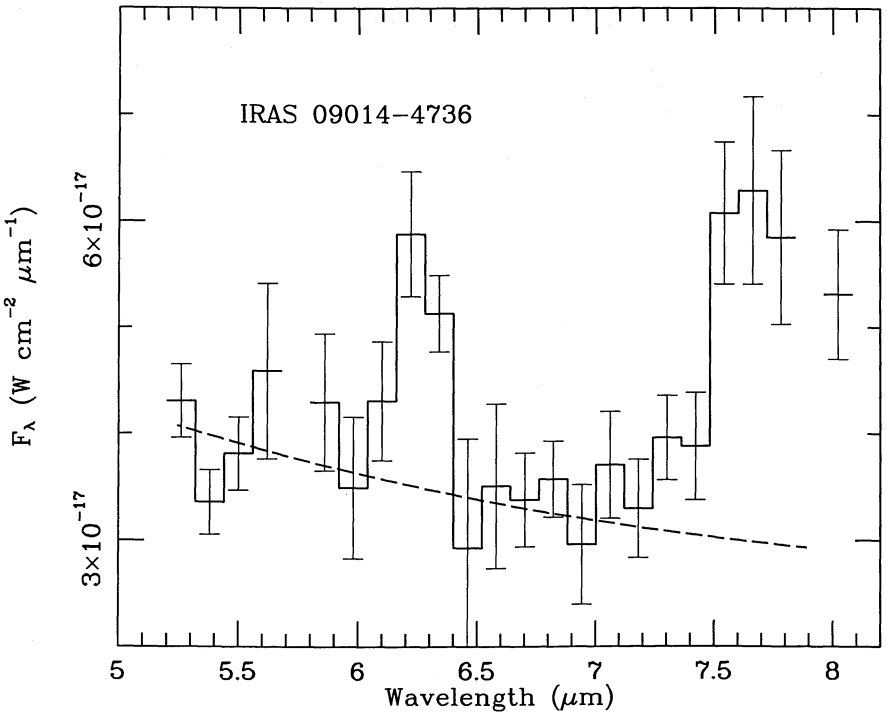

FIG. 14.—As Fig. 2, for the reflection nebula, IRAS 09014−4736

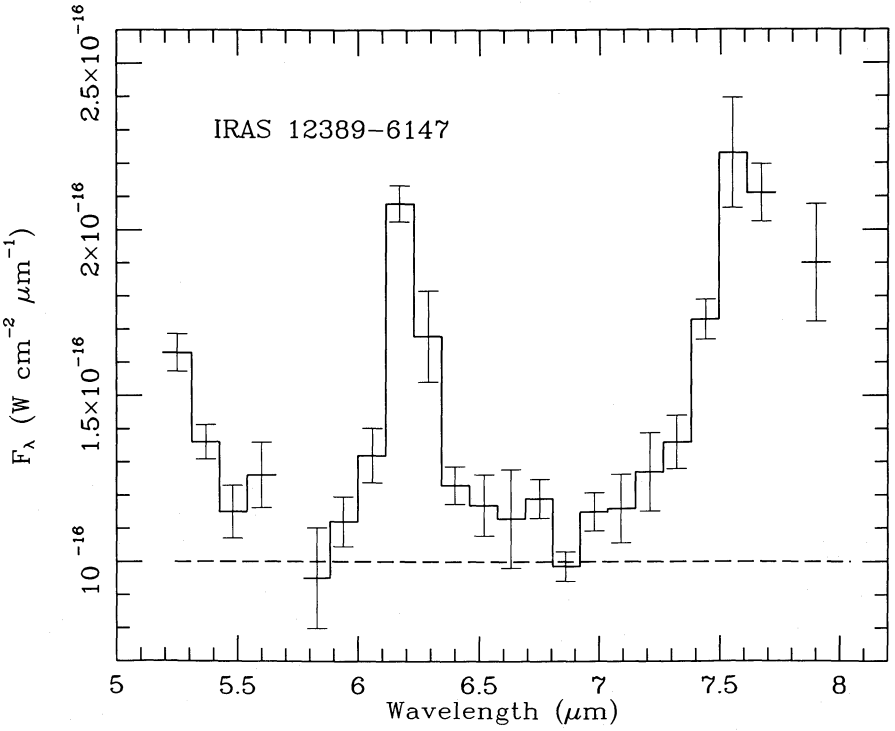

FIG. 15.—As Fig. 2, for the H II region, IRAS 12389−6147

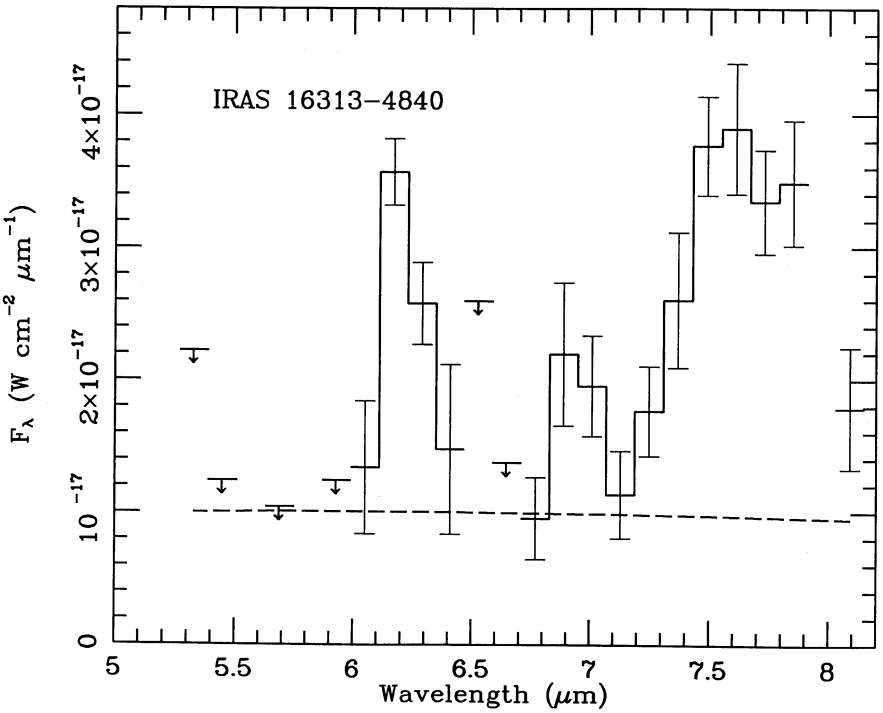

FIG. 16.—As Fig. 2, for the H II region, IRAS 16313−4840

elongated in about P.A. = 60°. It is completely invisible on the *J* photograph and appears as a tiny bipolar nebula in *R* and *I*. Its 5–8 μm spectrum, too (Fig. 16), is very red: no flux is detected in the continuum at our shortest wavelengths. The 6.2 μm feature may be somewhat red-shaded. Comparison of KAO and LRS spectra suggests that the infrared emission is spatially extended. There is a cross-reference in PSC2 to the SSSC, as X1631−486, whose fluxes exceed those of PSC2 by factors of 1.9 (12 μm) and 1.3 (25 μm), suggestive of PAH emission that is widely dispersed. Our interpolated continuum is set by splining between the LRS flux density at 10.0 μm and the observed KAO flux density near 6.7 μm.

o) IRAS 16396−4429

The photographic counterpart of this source is a small, extremely red, fan-shaped nebulous patch with a triangular brightish core, some 4″ by 3″, apex pointing in P.A. = 140°. There is evidence for a long-wavelength tail to the 6.2 μm band. The slightly elevated point at 7.0 μm may be a weak [Ar II] line. The splined continuum was set as for 16313−4840. The matching SSSC source, X1639−444, shows spatially extended 12 μm emission whose flux density exceeds that in PSC2 by 1.7. Our KAO spectrum (Fig. 17) also falls below the LRS level near 7.7 μm, confirming the likelihood of spatially dispersed PAH emission.

IV. INTEGRATED BAND FLUXES

In this section we calculate the integrated intensities of the emission features in our spectra and combine them with values derived from ground-based spectra or from the LRS for the 3.3 and 11.3 μm features. The complex of features near 3.4 μm and the 12.7 μm feature are not included since there are too few of the necessary high-resolution observations (Geballe *et al.* 1988; Roche, Aitken, and Smith 1988; Witteborn *et al.* 1988).

We adopted the methods of Paper I for the extent of the PAH feature at 6.2 μm, namely 6.0–6.6 μm. For the "7.7" μm band it was necessary to modify the technique in Paper I to cope with peaks significantly different from 7.7 μm by using twice the integrated flux between 7.3 μm and the actual peak (several objects peak at ∼7.6 μm, others not until 7.9–8.0 μm). This avoids both the necessity of taking two adjacent KAO spectra to cover the entire 7.7 μm structure and any confusion with the 8.7 μm feature on its flank. In all cases, these integrals were defined above the relevant interpolated continua. Likewise, the 6.9 μm band flux was obtained by integration above the splined continuum except for those objects where a broad plateau of emission links the 6.2 and 7.7 μm features, in which case we use the intervening higher level of plateau emission instead.

For HD 44179 (Paper I) and CPD −56°8032 (the present paper), our KAO data entirely include the combined 7.7/8.7 μm feature, and we were able to test for symmetry about the peak in the "7.7 μm" band in assessing the integrated flux. We found agreement to ≤10% for each of these two well-observed sources, justifying doubling the flux observed from the KAO between 7.3 μm and this peak.

To define the sharp bands in this manner, as distinct features above a broad continuum, is justified by the recent study of the Orion Bar (Paper II). In this region, the broad continuum that underlies the PAH bands does not show the same spatial distribution as the narrow features, indicative of separate sources and mechanisms of emission.

We have used radio continuum flux densities at 5 GHz (scaled down to a 22″ beam for sources with significant spatial extent in the radio continuum) to estimate the corrections to the integrated 3.3 and 7.7 μm band intensities (corrections were made to the latter band intensities before doubling the integrated fluxes) due to the Pfδ and (Pfα + Huβ) recombination

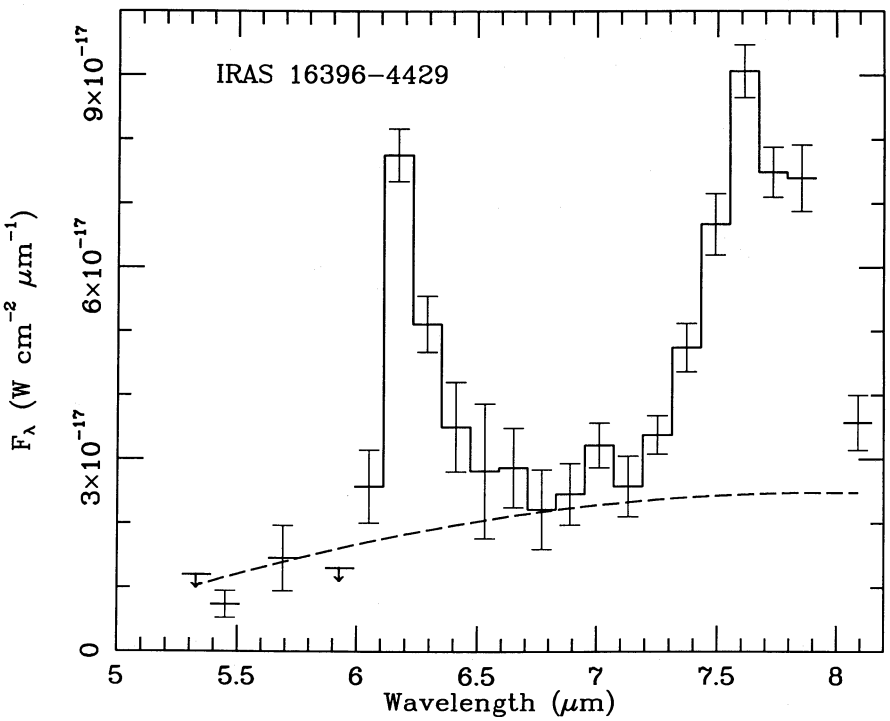

FIG. 17.—As Fig. 2, for the H II region, IRAS 16396−4429

lines (see Paper I), respectively, for CPD −56°8032, He 2–113, He 2–77, RCW 108, NGC 6302, and G333.6−0.2. All corrections were small relative to the relevant band intensities except those for the Pfα line of G333.6−0.2 and the Pfδ line of RCW 108. We could find no published information on radio continuum fluxes for the newly discovered *IRAS* sources nor for the *IRAS* peak within Cederblad 40, and we have made no adjustments for recombination line radiation to their estimated band intensities.

In Table 2 we summarize band intensities for emission features determined solely from our KAO spectra. The additional 3.3 μm band data (see notes to Table 2) refer to pointlike infrared objects except for He 2–77, RCW 108, and IRAS 05044−0325; we have rescaled these three measurements to our 22″ aperture to define relative band intensities (see below), assuming uniform surface brightness in the KAO beam. Estimates of the 11.3 μm feature strength relative to the 7.7 were made by normalizing the LRS spectra of the objects to the KAO data in the overlap region near 8 μm. We applied the same methods to the sources in Paper I so that we can place all our objects on the same footing. For some reflection nebulae, KAO spectra in different locations show significant variations in the PAH bands. For such sources we have not included rescaled 11.3 μm band data since we cannot decide which KAO spectrum to use for normalization. This affects IRAS 05044−0325 alone among the southern objects, and NGC 2023, NGC 2071, and Parsamian 18 from Paper I. Distances are not yet known to most of the newly observed sources. Therefore, we have directly compared the apparent 6.2 and 7.7 μm band intensities for new sources and have combined these data with those implicit in Paper I for the northern sample of 5–8 μm spectra.

We have assigned objects to three categories of nebular type: planetaries, reflection nebulae, and H II regions, based on several criteria: (1) optical spectra, when available; (2) nebular morphology and the existence of *IRAS* SSSC sources that indicate the reflection nature of some nebulae; (3) the longest wavelength *IRAS* color temperatures that sharply discriminate between planetaries and the other two types (planetaries have 60-to-100 μm color temperatures >100 K; reflection nebulae and H II regions show values ∼50 K). We included protoplanetaries with the planetaries. Table 2 includes our nebular types.

In Figure 18 we correlate the 6.2 and 7.7 μm band intensities for the 22 northern sources of Paper I, and the 18 southern sources or locations of the present paper. The conspicuous trend has a correlation coefficient, r^2, of 0.84 (for 18 objects of the southern sample alone) or 0.86 (for all 40 sources, or separate locations within a source detected in both bands, in northern and southern sources). We have fitted a straight line to the points in Figure 18 by least-squares techniques, and we have also treated the new southern data separately from the entire sample. Our estimates for slope and intercept, including rms errors in these coefficients, are derived by considering both axes to be subject to errors of measurement. We find for the 18 southern sources alone

$$\log_{10} I(7.7\ \mu\text{m}) = (1.04 \pm 0.11) \log_{10} I(6.2\ \mu\text{m}) + (0.37 \pm 0.24)\,,$$

and for all 40 sources

$$\log_{10} I(7.7\ \mu\text{m}) = (1.02 \pm 0.07) \log_{10} I(6.2\ \mu\text{m}) + (0.31 \pm 0.16)\,.$$

These results agree well with those of Paper I for which the corresponding parameters were 1.05 ± 0.22 and 0.25 ± 0.21 (from band luminosities) or 1.02 ± 0.15 and 0.26 ± 0.18 (from a reanalysis of apparent band intensities).

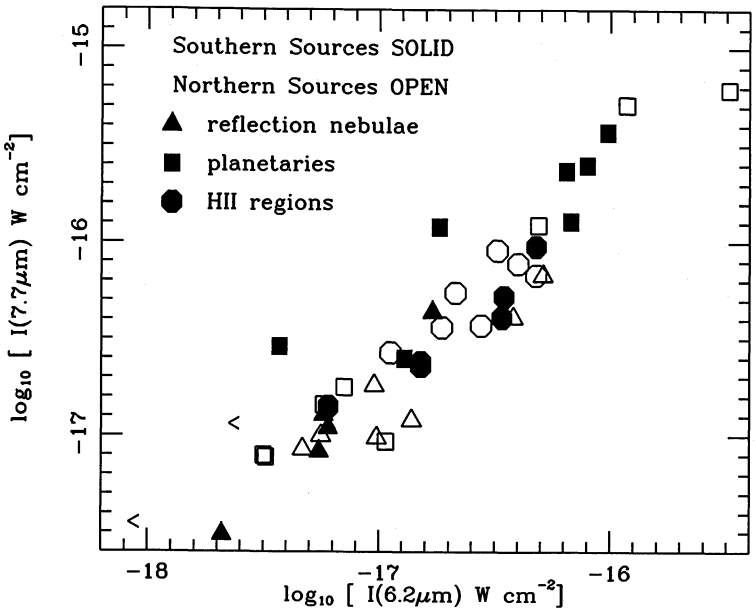

FIG. 18.—Correlation between the intensities of the 6.2 and 7.7 μm emission bands, distinguishing sources described in Paper I (*open symbols*) and in the present southern survey (*solid symbols*), and separating sources by nebular type. The two 6.2 μm upper limits correspond to the northern planetaries, M 4-18 and NGC 6572.

We conclude again that the 6.2 and 7.7 μm bands are very well correlated with formal best-fit ratio of $I(7.7)/I(6.2) \sim 2.0(+1.0, -0.6)$. The linear relationship between these two features is noteworthy, demonstrating again that these bands have a common carrier.

The "new" 5.2 μm feature was present in quite a number of the northern KAO spectra (Paper I), although, because of its location at the extreme edge of the spectra, we did not call attention to it in Paper I. Its strength is correlated with that of the 7.7 μm feature in Figure 19. We omit two sources from Figure 19, HR 4049 and IRAS 09014−4736, because we have only upper limits to the 5.2 μm bands. There is clearly a correlation between the intensities of the two bands, although it is noisier than the corresponding plot relating the 6.2 and 7.7 μm features probably, in part, because of the greater uncertainties in defining the much weaker 5.2 μm band intensity and because of its location at the edge of our spectra. We find for 33 sources

$$\log_{10} I(7.7\ \mu\text{m}) = (0.92 \pm 0.11) \log_{10} I(5.2\ \mu\text{m}) - (1.39 \pm 0.18)\ ,$$

suggesting that both bands are correlated, with formal best-fit value of $I(7.7)/I(5.2) \sim 24(+13, -8)$. Consequently, this new feature also belongs to the "generic" spectrum of infrared bands.

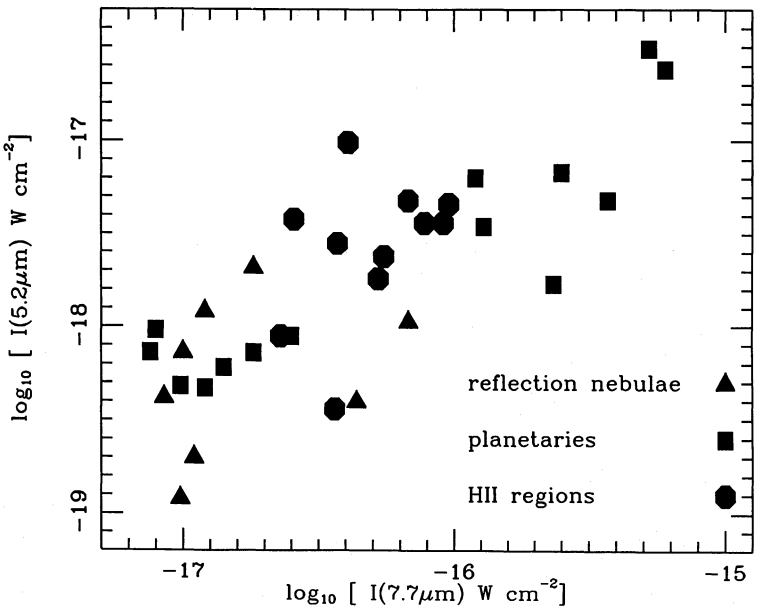

FIG. 19.—Correlation between the new 5.2 μm band and that at 7.7 μm, distinguishing sources by nebular type

TABLE 3

AVERAGE RELATIVE INTENSITIES[a] OF BANDS OBSERVABLE FROM THE KAO WITH RESPECT TO $I(7.7)$

	RELATIVE INTENSITIES			
SAMPLE	$I(5.2)/I(7.7)$ 1–13[b]	$I(5.6)/I(7.7)$ 0.4–16[b]	$I(6.2)/I(7.7)$ 13–83[b]	$I(6.9)/I(7.7)$ 0.5–26[b]
Northern:				
PN	3.5 ± 0.9	7.3 ± 3.2	49 ± 10	...
RN	6.1 ± 1.8	10.2 ± 1.5	77 ± 10	16.4 ± 4.0
H II	6.2 ± 1.6	7.0 ± 1.6	52 ± 6	...
Southern:				
PN	3.5 ± 1.4	None	31 ± 6	...
RN	0.9	0.5:	54 ± 6	None
H II	9.8 ± 5.7	3.3 ± 2.3	64 ± 5	...
Whole sample:				
PN	3.5 ± 0.9	7.3 ± 3.2	41 ± 6	...
RN	5.4 ± 1.7	9.0 ± 1.8	68 ± 7	16.4 ± 4.0
H II	7.5 ± 2.2	5.8 ± 1.4	58 ± 4	...
All sources	5.4 ± 1.1	7.3 ± 1.1	54 ± 4	16.4 ± 4.0

[a] In percent.
[b] Range in percent.

Two weak features were shown in Paper I to belong to the generic PAH spectrum, namely the 5.6 and 6.9 μm bands. In Tables 3 and 4 we present the average ratios of these bands, of the 3.3, and of the new 5.2 μm feature relative to the intensity of the 7.7 μm feature, separating northern, southern, and combined samples. Table 3 summarizes data solely for those bands that can be observed in our KAO spectra, and Table 4 includes the 3.3 and 11.3 μm data obtained as described above. We caution that average relative intensities for the weak bands can be highly misleading. When present, the 5.6 μm band may attain an average strength ~10% that of the 7.7 μm band (Paper I), but this feature is entirely absent from the KAO spectra of many objects. Consequently, Tables 3 and 4 also offer the total ranges of variation in these ratios, defined from the combined sample of sources; we further separate average strengths for different nebular types.

TABLE 4

AVERAGE RELATIVE INTENSITIES[a] OF BANDS UNOBSERVABLE FROM OUR KAO SPECTRA WITH RESPECT TO $I(7.7)$

	RELATIVE INTENSITIES	
SAMPLE	$I(3.3)/I(7.7)$ 1–12[b]	$I(11.3)/I(7.7)$ 7–87[b]
Northern:		
PN	6.9 ± 1.3	47 ± 9
RN	8.0 ± 0.9	30 ± 15
H II	13.6 ± 2.8	35 ± 7
Southern:		
PN	5.2 ± 2.6	9 ± 1
RN	3.3 ± 2.2	17 ± 1
H II	11.4 ± 2.9	24 ± 3
Whole sample:		
PN	6.3 ± 1.3	29 ± 7
RN	5.7 ± 1.7	22 ± 5
H II	13.0 ± 2.2	30 ± 4
All sources	8.4 ± 1.2	29 ± 4

[a] In percent.
[b] Range in percent.

V. DISCUSSION

a) General Comments

Most of the northern and southern spectra show a feature near 5.2 μm, implying its reality. Since many PAHs show a C–H overtone near this wavelength, its discovery further strengthens the general identification of all the bands with these types of molecule.

All three of the rare protoplanetaries that we have studied, namely Roberts 22, HR 4049, and HD 44179 (in Paper I), show PAH emission features.

There is no correlation between the plateau of emission that underlies the 6.2 and 7.7 μm bands and nebular type, C/O ratio in planetaries, *IRAS* color temperatures, ratio of $I(6.2)/I(7.7)$, or even the 11–13 μm plateau. The 6–9 μm plateau of emission probably originates in PAH clusters containing several hundred carbon atoms. The relative populations of PAHs that emit the narrow features and the larger moieties that produce the broad, underlying continuum are expected to vary considerably from source to source. For example, in objects that produce the emitting material (e.g., protoplanetaries and planetaries) these relative proportions will depend on pressure, temperature, density, and outflow velocity in the PAH formation zone (Allamandola, Tielens, and Barker 1988). Where the PAHs reside in a molecular cloud prior to excitation by a local source (e.g., in reflection nebulae and H II regions), we again expect the proportions to vary greatly, driven by source to source differences in typical energy of the radiation field and photon flux, and internal extinction. Consequently, our failure to correlate the 6–9 μm plateau with any obvious single parameter is, perhaps, not surprising.

Several spectra show evidence for a red shading of the 6.2 μm band. Some caution is warranted, however, since the width of this emission feature is comparable to our resolution. Nevertheless, *IRAS* 16396−4429 and G333.6−0.2 are such striking examples of this phenomenon that it may well be real. Higher resolution studies of these bands are needed to confirm the red degradation. However, we note that such shading may be caused by anharmonicity; i.e., the $v = 2 \rightarrow 1$ and $3 \rightarrow 2$ emission in this mode is shifted to slightly longer wavelengths (Barker, Allamandola, and Tielens 1987).

b) Variations in the Generic Band Spectrum

Tables 3 and 4 reveal the following significant results that give insight into physical conditions in different nebular types. We draw the following conclusions from the rows in Tables 3 and 4 marked "whole sample" which use the entire sample (from Paper I and the present paper) of objects, separated by nebular type. (1) Planetaries have larger 7.7 μm band intensities relative to 6.2 μm than either H II regions or reflection nebulae which are indistinguishable from one another by this ratio. (2) H II regions clearly show the strongest 3.3 μm features. (3) The 5.2 μm band is weakest in planetaries. (4) Planetaries show the strongest 11.3 μm bands. We can find no pattern of occurrence for the 5.6 μm band with respect to nebular type. It should be noted that the 6.9 μm feature can be lost in some planetaries and H II regions to the 6.98 μm [Ar II] line; it can only be reliably assessed in our spectra if there is a broad feature (two adjacent comparably strong detectors) at this wavelength. Consequently, we shall quantify the 6.9 μm band strength only in reflection nebulae where it can be highly conspicuous. The final lines in Tables 3 and 4 summarize the

means for all these bands relative to that at 7.7 μm, without regard to nebular type.

The ratio $I(6.2)/I(7.7)$ is interesting in that it clearly discriminates between circumstellar material (created in and excited by the planetaries) and interstellar (ambient matter influenced by mere proximity to hot stars as in both reflection and ionized environments). It seems that planetaries, which are embedded in synthesized material, contain a slightly different PAH family than the interstellar medium. Perhaps this is the result of shock destruction and/or ultraviolet photoisomerization in the interstellar medium which will tend to weed out the less stable PAHs (Crawford, Tielens, and Allamandola 1985). The 6.2 and 7.7 μm modes are so close together in energy that excitation variations should have only a minor influence on $I(6.2)/I(7.7)$. Consequently, this ratio should reflect the intrinsic strengths of these modes.

That H II regions have the strongest 3.3 μm bands and reflection nebulae the most obvious 6.9 μm bands may have similar causes. The 3.3 μm feature corresponds to the highest energy, fundamental vibration in a PAH. This will be most highly excited with respect to the longer wavelength fundamentals if either the number of carbon atoms in the emitter is small, or the ultraviolet photon energy that excites the PAHs is large (Allamandola, Tielens, and Barker 1985). The relatively strong 3.3 μm band in H II regions, compared with reflection nebulae and planetaries, implies either that higher energy photons are more plentiful in H II regions, or that smaller PAHs are more abundant in H II regions. We suspect that Lyα photons are largely responsible for the high level of PAH excitation in H II regions.

The conspicuous presence of the 6.9 μm band in reflection nebulae may also owe its explanation to PAH stability and photon field energy. The 6.9 μm band can arise from the less symmetric, noncompact PAHs such as chrysene (Allamandola, Tielens, and Barker 1985, 1987) which are also the less stable forms (Crawford, Tielens, and Allamandola 1985; van der Zwet and Allamandola 1985). Alternatively, the CH deformation vibration in aliphatic sidegroups such as CH_2 and CH_3 attached to a PAH may be responsible (Duley and Williams 1981; de Muizon *et al.* 1986; Tielens and Allamandola 1987). In either case, the carriers are not as photostable as compact, symmetric PAHs with respect to high-energy photons. One would, therefore, expect that these less stable molecules would survive longer in the more benign regions of a reflection nebula than in the higher energy photon field of an H II region or planetary nebula (see Geballe *et al.* 1988). The aliphatic sidegroup explanation can be tested observationally, since the groups have bands in the 3.3–3.5 μm region as well. If the 6.9 μm band arose from $-CH_2$ and $-CH_3$ groups, one would expect correlated behavior with one or more of the features between 3.3 and 3.5 μm.

We do not yet know the intrinsic 5.2 μm band intensities for isolated PAHs since quantitative laboratory spectra are hard to obtain. Therefore, we have no explanation for the relative weakness of this band in planetaries, although we suspect that this feature contains structural information about the molecules.

The substantial variations among planetaries in $I(11.3)/I(7.7)$ merit comment. First, some of these ratios based on normalizing the LRS spectra are quite different values than we tabulated in Paper I on the basis of attempting to scale ground-based small aperture data up to the KAO 22″ aperture. We feel that ratios derived from the LRS are likely to be more reliable than those in Paper I and note that the LRS–based values deduced are invariably greater than those in Paper I, as if the increased aperture of the LRS has preferentially included more 11.3 μm emission than 7.7 μm emission. This effect seems to occur only for the 11.3 μm band and only in the planetaries. Second, there are striking differences in $I(11.3)/I(7.7)$ between northern and southern samples of planetaries. All the southern nebulae have much weaker 11.3 μm features than the northern, perhaps reflecting the strong bias among southern objects toward compact, young, planetaries and protoplanetaries. We speculate that strong 11.3 μm emission demands a fully fledged planetary which may signify that this emission is concentrated around the peripheries of planetary nebulae, in the neutral zones (see Aitken and Roche 1983; Bentley *et al.* 1984).

The ratio of $I(11.3)/I(3.3)$ has been used to determine the likely number of carbon atoms in the emitting PAH molecules (see Allamandola, Tielens, and Barker 1985; de Muizon *et al.* 1986). However, large PAHs will not contribute as much to the intensity of the 3.3 μm band as to the 11.3 μm band (Allamandola, Tielens, and Barker 1988), rendering the ratio of these two bands somewhat ambiguous. Further, we urge great caution in the use of $I(11.3)/I(3.3)$ when it involves scaling small aperture ground-based measurements up to the LRS spectra. For this reason, we do not tabulate this ratio.

An important pattern concerning the peak wavelength of the "7.7" μm feature also emerges from the KAO spectra that again may discriminate between locally made PAHs and ambient interstellar molecules. Dubbing the most intense feature as "the 7.7 μm band" is misleading. The peak of this feature varies considerably, probably indicative of different components dominating the emitting species in different environments. One might contrast, for example, the planetary CPD −56°8032 (Fig. 2, 7.9 μm peak), the H II region RCW 108 (Fig. 6, 7.65 μm), and the reflection nebula IRAS 08513−4201 (Fig. 13, 7.7 μm). A similar contrast is to be found between the protoplanetary nebula HD 44179 (Paper I, 7.9 μm peak) and the Orion Bar (Paper II, 7.6 μm). Table 5 summarizes the best-determined peak wavelengths (from spectra with the highest signal-to-noise or in which the absence of information in detector 23 does not compromise the estimation of the peak) of this band among the three types of nebulae, based on Paper I and the present paper. The "7.7" μm peak in planetaries is significantly longer than in other nebular environments, as evidenced by an examination of the peak wavelengths in Table 5.

High-resolution FOGS spectra of several PAH sources suggest the existence of two separate components within the "7.7" μm feature, one from species that have an intense fundamental between ~7.5 and 7.6 μm, and a second from species with fundamentals between 7.8 and 8.2 μm (e.g., Bregman *et al.* 1987). The variations in peak wavelength might, therefore, represent changes in dominance of these two components, perhaps due to two independent molecules or classes of molecule. Further high-resolution studies of the sources described in the present paper may provide more insight into this issue. In particular, it might eventually prove possible to place significant constraints on the geometries of the dominant PAH species in different nebulae.

c) *The Bands and* C/O *Ratios in Planetaries*

One particularly important result from Paper I is the relation for planetaries between gas phase C/O ratio and the relative importance of PAH emission as compared with grain emission, quantified by $f(7.7)$, the fraction of total *IRAS* emis-

TABLE 5

ACTUAL PEAK WAVELENGTH OF THE "7.7" MICRON BAND IN DIFFERENT NEBULAE WITH GOOD DETERMINATIONS

Object	Peak
Planetaries	
J 900	7.7
M 1-11	7.7
BD +30°3639	7.8–8.0
IC 5117	7.7–8.0
HD 44179	7.85
NGC 7027	7.6, 7.8[a]
CPD −56°8032	7.9
He 2–113	7.8–8.0
Roberts 22	7.8–8.0
MWC 922	7.7–7.9
HR 4049	7.7
Reflection Nebulae	
P18-1	7.4–7.7
P18-2	7.55
P18-3	7.6
NGC 7023	7.6
05044−0325pk	7.65
08513−4201	7.7
NGC 2023	7.6
H II Regions	
Ori Bar (All 4 positions)	7.65
SAO 161375	7.7–7.9
RCW 108	7.65
16396−4429	7.6
GL 437	7.65

[a] Two components seen at high spectral resolution

sion radiated by the 7.7 μm feature. From the present southern sample we can readily incorporate NGC 6302, with its C/O of 0.2, into this trend, although the powerful [Ne VI] line renders our estimate of 7.7 μm band strength somewhat difficult. Consequently, we plot NGC 6302 in Figure 20 as two connected points, representing two extreme methods of calculating the underlying 7.7 μm band intensity. Of greatest interest would be the inclusion of the [WC 10] planetary nuclei in such a figure because of their qualitatively carbon-rich appearance. However, only CPD −56°8032 has been adequately studied with *IUE* and only a preliminary estimate exists in the literature for C/H in this nebula (Houziaux and Heck 1982). We have obtained copies from the *IUE* data base via NSSDC of several more ultraviolet spectra of CPD −56°8032 which we have analyzed with respect to C/O. *IUE* spectra of He 2–113 are too poor for C/O analysis.

These [WC 10] objects offer the prospect of relatively easy determination of C/O because of the extremely low excitation, in particular the absence of [O III] in both optical (see Webster and Glass 1974) and *IUE* spectra. Consequently, we may approximate $N(C)/N(O) = \{N(C^+) + N(C^{++})\}/N(O^+)$. Unfortunately we do not have accurate values of T_e or N_e in CPD −56°8032; for T_e we adopt 10^4 K (as did Houziaux and Heck 1982 from "the general appearance of the spectrum"); for N_e we adopt 10^4 cm^{-3}, typical of other [WC 10] nebulae (e.g., M 4-18; Goodrich and Dahari 1985). Normally, we would use the red [S II] doublet line ratio for N_e, but in CPD −56°8032 the λ6731 line is severely blended with C III and C II lines. Table 6 summarizes the *IUE* spectra and line information for the C III] λ1909, C II] λ2326, and [O II] λ2470 lines which we will utilize for our estimate of C/O. We note that our estimated line fluxes differ significantly from *IUE* spectrum to spectrum, although the relative intensities change much less. However, we cannot reproduce the line fluxes given by Houziaux and Heck in their final table even for the pair of *IUE* spectra they cite. We include Barlow's value for the observed Hβ flux (as cited by

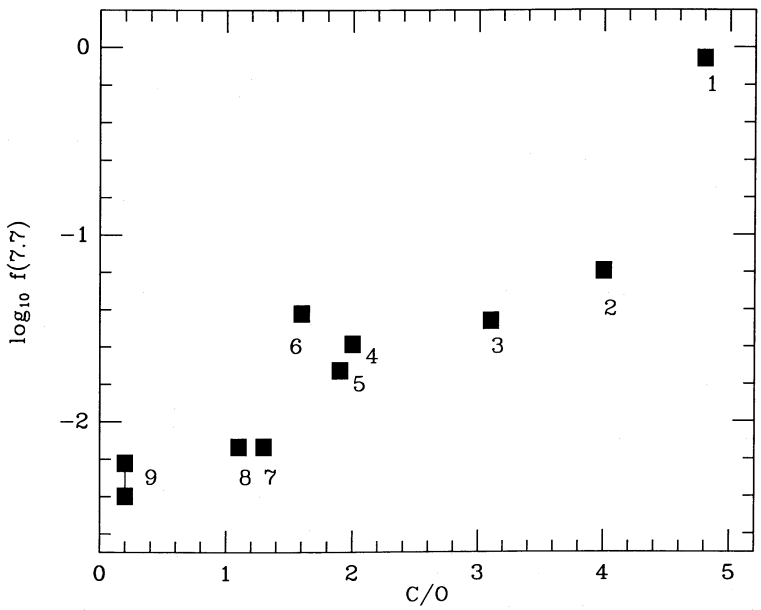

FIG. 20.—The correlation between fraction of total *IRAS* emission radiated by the dominant 7.7 μm band and gas phase C/O ratio for nine planetaries or protoplanetaries. Key: 1, CPD −56°8032; 2, J900; 3, NGC 7027; 4, HR 4049; 5, IC 5117; 6, BD +30°3639; 7, IC 418; 8, NGC 6572; 9, NGC 6302 (the two points for this nebula indicate extreme ways of extracting the 7.7 μm PAH feature from the [Ne VI] line and represent the uncertainty).

TABLE 6

IUE SPECTROSCOPY OF CPD −56°8032 WITH C AND O LINE FLUXES

Line	Spectrum	Observed Flux[a]	Exposure (minutes)	Average Observed Flux[a]	Average Intrinsic Flux[a]
1909	SWP 6718	5.99E − 13	20		
	SWP 8947	4.80E − 13	55		
	LWR 5733	2.67E − 12	10		
	LWR 7187	1.13E − 12	20		
	LWR 7700	6.53E − 13	25		
Average				11.6 ± 3.0E − 13	10.0 ± 2.6E − 11
2326	LWR 5733	1.40E − 12	10		
	LWR 7187	9.03E − 13	20		
	LWR 7700	5.54E − 13	25		
Average				9.5 ± 1.6E − 13	10.5 ± 1.7E − 11
2470	LWR 5733	2.98E − 13	10		
	LWR 7187	7.21E − 14	20		
	LWR 7700	1.13E − 13	25		
Average				1.6 ± 0.5E − 13	9.2 ± 2.9E − 12
4861	Barlow			1.12E − 12	8.31E − 12

[a] All fluxes are in ergs $cm^{-2} s^{-1}$.

Aitken *et al.* 1980) and correct all the line fluxes for an A_v of 1.86 (see Houziaux and Heck 1982) using Seaton's (1979) ultraviolet extinction law. The absence of any conspicuous P Cygni absorption profiles attached to the relevant lines of CPD −56°8032 suggests that we may attribute the lines we measure to the nebula and not to the stellar wind.

We converted our intrinsic line fluxes with respect to Hβ into ionic abundances following the formulation of Harrington *et al.* (1980) for collisional excitation rate coefficients and averaged strengths, branching ratio (0.201; Zeippen 1982), and effective rate coefficient (equivalent to a factor of 3.44 for our adopted T_e and N_e) for the λ2470 transition. These yielded $N(C^+)/N(H^+) = 1.3E-3$, $N(C^{++})/N(H^+) = 3.0E-3$, and $N(O^+)/N(H^+) = 9.6E-4$, whence we approximate $N(C)/N(O) = \{N(C^+) + N(C^{++})\}/N(O^+) \sim 4.8$. Following the 1 σ errors in observed mean line fluxes through the calculation yields C/O ∼ 4.8(+3.3, −2.2).

Figure 20 updates the figure from Paper I that plots $f(7.7)$ versus C/O in planetaries to include NGC 6302, HR 4049, and CPD −56°8032. It differs from the version in Paper I in that we have now recalculated the total fluxes observed by *IRAS* based on the modified data in PSC2. To incorporate HR 4049 we have used the flux in the 7.7 μm band divided by that of its 1250 K blackbody dust component (described by Lamers *et al.* 1986 as dominating the infrared spectrum) to represent the ordinate and Lambert *et al.*'s (1988) estimate of C/O ∼ 2 (corresponding to $T_{\rm eff} = 8500$ K) for the abscissa. One final difference is that we have replaced the C/O used for BD +30°3639 in Paper I (2.8) by the more recent determination due to Pwa, Pottasch, and Mo (1986), of C/O = 1.6. We see that the same trend is visible in the enlarged data set, *again indicating a hydrocarbon carrier for the emission features* (see Paper I).

Although we have no quantitative estimate for C/O in the protoplanetary nebula, Roberts 22, we note the existence of an OH maser in the circumstellar envelope (Allen *et al.* 1982). However, the presence of the PAH bands may argue for a carbon-rich environment closer to the star. Comparison with other protoplanetaries such as the [WC 9] object, Sw St 1 (=HD 167362), suggests that some time is required before the carbon-rich stellar wind is capable of altering the chemistry of the nebular envelope. Sw St 1 contains a [WC 9] nucleus, yet its gas phase C/O is only 0.7 (Flower, Goharji, and Cohen 1984), and it shows no PAH features in the 8–13 μm spectrum by Aitken and Roche (1982), but instead a smooth silicate emission feature. A general detailed comparison of all properties of the very low excitation protoplanetaries promises some understanding of the way in which dust condenses in these nebulae and of the changes in envelope chemistry with evolutionary phase.

d) Spatially Extended PAH Emission

When we have found matches in the SSSC for our observed *IRAS* sources, it is generally the case that the degree of enhancement of flux density is greatest for the 12 μm band. This, we suggest, indicates that there is often spatially extended PAH emission since the influence of the PAH features on the *IRAS* bands is greatest through the 12 μm filter.

e) Longer Wavelength Features

Finally, we note that in the *IRAS* LRS spectra of several of the objects in our total sample of sources, the long-wavelength LRS spectrum (from about 14 to 23 μm) shows definite convexity, too sharp to be a blackbody. The apparent bumps do not correspond to known atomic lines, and we feel that these must represent other bending modes of PAH molecules, as for example described by Allamandola, Tielens, and Barker (1987). A good example of one such source is He 2–113 = Hen 1044 whose LRS spectrum was reproduced by CTA (their Fig. 1).

Note added in manuscript (*1989 January 10*).—A recent analysis of the C/O abundance ratio in NGC 6302 by M. J. Barlow (private communication) based on a consideration of the highest relevant ionization stages of carbon and oxygen suggests that C/O in this nebula is greater than 0.2 but strictly less than 0.9. Consequently, this nebula retains its significance in Figure 20 as the object with the lowest C/O ratio and the lowest value of $f(7.7)$ in our trend.

We thank the staff of the KAO and Northrop Services for their valuable assistance during the southern hemisphere expeditions and the US Navy for their support at the Operation Deepfreeze station in Christchurch, New Zealand. We are grateful to the Director of MSSSO for providing time on the 2.3 m telescope in Australia for us to observe several of these *IRAS* sources, and to Peter McGregor and Michael Ashley for helping us with the observations using their own spectrometer. M. C. acknowledges support from NASA's Airborne Astronomy program through cooperative agreement NCC 2–142 between NASA-Ames Research Center and University of California, Berkeley. We are grateful to the National Space Science Date Center at the NASA Goddard Space Flight Center for providing *IUE* archival data on CPD −56°8032, and to Terry Armitage for his assistance in expediting our remote inspection of archival *IUE* spectra of CPD −56°8032 and He 2–113 at the Colorado RDAF. We also thank Tom Geballe for his careful reading of the original paper.

REFERENCES

Aitken, D. K., Barlow, M. J., Roche, P. F., and Spenser, P. M. 1980, *M.N.R.A.S.*, **192**, 679.
Aitken, D. K., and Jones, B. 1974, *M.N.R.A.S.*, **167**, 11P.
———. 1975, *M.N.R.A.S.*, **172**, 141.
Aitken, D. K., and Roche, P. F. 1982, *M.N.R.A.S.*, **200**, 217.
———. 1983, *M.N.R.A.S.*, **202**, 1233.
Allamandola, L. J. 1987, in *Polycyclic Aromatic Hydrocarbons and Astrophysics*, ed. A. Leger, L. d'Hendecourt, and N. Boccara (Dordrecht: Reidel), p. 343.
Allamandola, L. J., Bregman, J. D., Sandford, S. A., Witteborn, F. C., Wooden, D. H., and Rank, D. M. 1989, in preparation (Paper IV).
Allamandola, L. J., Tielens, A. G. G. M., and Barker, J. R. 1985, *Ap. J. (Letters)*, **290**, L25.
———. 1987, in *Physical Processes in Interstellar Clouds*, ed. G. E. Morfill and M. Scholer (Dordrecht: Reidel), p. 305.
———. 1988, *Ap. J.*, submitted.
Allen, D. A. 1973*a*, *M.N.R.A.S.*, **161**, 145.
———. 1973*b*, *M.N.R.A.S.*, **168**, 1.
———. 1987, private communication.
Allen, D. A., Baines, D. W. T., Blades, J. C., and Whittet, D. C. B. 1982, *M.N.R.A.S.*, **199**, 1017.
Allen, D. A., Hyland, A. R., and Caswell, J. L. 1980, *M.N.R.A.S.*, **192**, 505.
Aller, L. H., Ross, J. E., O'Mara, B. J., and Keyes, C. D. 1981, *M.N.R.A.S.*, **197**, 95.
Ashley, M. C. B., and Hyland, A. R. 1988, preprint.
Barker, J. B., Allamandola, L. J., and Tielens, A. G. G. M. 1987, *Ap. J. (Letters)*, **315**, L61.
Barlow, M. J. 1983, in *IAU Symposium 103, Planetary Nebulae*, ed. D. R. Flower (Dordrecht: Reidel), p. 105.
Barral, P., Canto, J., Meaburn, J., and Walsh, J. R. 1982, *M.N.R.A.S.*, **199**, 817.
Bentley, A. F., Hackwell, J. A., Grasdalen, G. L., and Gehrz, R. D. 1984, *Ap. J.*, **278**, 665.
Bregman, J. D., Allamandola, L. J., Tielens, A. G. G. M., Geballe, T., and Witteborn, F. C. 1988, *Ap. J.*, submitted (Paper II).
Bregman, J. D., Allamandola, L. J., Tielens, A. G. G. M., Witteborn, F. C., Rank, D. M., and Wooden, D. 1987, in *Proc. Summer School on Interstellar Processes, Abstracts of Contributed Papers*, ed. D. J. Hollenbach and H. A. Thronson (NASA TM 88342), p. 117.
Bregman, J. D., Dinerstein, H. L., Goebel, J. H., Lester, D. E., Witteborn, F. C., and Rank, D. M. 1983, *Ap. J.*, **274**, 666.
Cohen, M. 1975, *M.N.R.A.S.*, **173**, 489.
Cohen, M., Allamandola, L. J., Tielens, A. G. G. M., Bregman, J., Simpson, J. P., Witteborn, F. C., Wooden, D., and Rank, D. M. 1986, *Ap. J.*, **302**, 737 (Paper I).
Cohen, M., and Barlow, M. J. 1980, *Ap. J.*, **238**, 585.
Cohen, M., and Jones, B. F. 1987, *Ap. J. (Letters)*, **321**, L151.
Cohen, M., and Tielens, A. G. G. M. 1989, in preparation.
Cohen, M., Tielens, A. G. G. M., and Allamandola, L. J. 1985, *Ap. J. (Letters)*, **299**, L93 (CTA).
Crawford, M. K., Tielens, A. G. G. M., and Allamandola, L. J. 1985, *Ap. J. (Letters)*, **293**, L45.
Danziger, I. J., Frogel, J. A., and Persson, S. E. 1973, *Ap. J. (Letters)*, **184**, L29.
de Muizon, M., Geballe, T. R., d'Hendecourt, L. B., and Baas, F. 1986, *Ap. J. (Letters)*, **306**, L105.
de Muizon, M., d'Hendecourt, L. B., and Geballe, T. R. 1987, in *Polycyclic Aromatic Hydrocarbons and Astrophysics*, ed. A. Leger, L. d'Hendecourt, and N. Boccara (Dordrecht: Reidel), p. 287.
de Muizon, M., Preite Martinez, A., and Heydari-Malayeri, M. 1987, in *Planetary and Proto-Planetary Nebulae: From IRAS to ISO*, ed. A. Preite Martinez (Dordrecht: Reidel), p. 185.
Duley, W. W., and Williams, D. A. 1981, *M.N.R.A.S.*, **196**, 209.
Flower, D. R., Goharji, A., and Cohen, M. 1984, *M.N.R.A.S.*, **206**, 293.
Frogel, J. A., and Persson, S. E. 1974, *Ap. J.*, **192**, 351.
———. 1975, *Ap. J.*, **197**, 351.
Geballe, T. R., Lacy, J. H., Persson, S. E., McGregor, P. J., and Soifer, B. T. 1985, *Ap. J.*, **292**, 500.
Geballe, T. R., Tielens, A. G. G. M., Allamandola, L. J., Moorhouse, A., and Brand, P. W. J. L. 1988, *Ap. J.*, submitted.
Goodrich, R. W., and Dahari, O. 1985, *Ap. J.*, **289**, 342.
Harrington, J. P., Lutz, J. H., Seaton, M. J., and Stickland, D. J. 1980, *M.N.R.A.S.*, **191**, 13.
Houziaux, L., and Heck, A. 1982, in *IAU Symposium 99, Wolf-Rayet Stars: Observations, Physics, Evolution*, ed. C. W. H. de Loore and A. J. Willis (Dordrecht: Reidel), p. 139.
IRAS catalogs and atlases: Point Source Catalog. 1985 (Washington, DC: US Government Printing Office).
IRAS Small Scale Structure Catalog. 1986, Joint IRAS Science Working Group ed. G. Helou, and D. W. Walker (Washington DC: US Government Printing Office) (SSSC).
IRAS Low Resolution Spectral Atlas. 1986, IRAS Science Team, *Astr. Ap. Suppl.*, **65**, 1 (LRS).
Lambert, D. L., Hinkle, K. H., and Luck, R. E. 1988, preprint.
Lamers, H. J. G. L. M., Waters, L. B. F. M., Garmany, C. D., Perez, M. R., and Waelkens, C. 1986, *Astr. Ap.*, **154**, L20.
Leger, A., and Puget, J. L. 1984, *Astr. Ap.*, **137**, L5.
Lester, D. E., and Dinerstein, H. L. 1984, *Ap. J. (Letters)*, **281**, L67.
Manchester, R. N., Goss, W. M., and Robinson, B. J. 1969, *Ap. Letters*, **3**, 11.
Merrill, K. M., and Stein, W. A. 1976, *Pub. A.S.P.*, **88**, 285.
Payne, H. E., Phillips, J. A., and Terzian, Y. 1988, *Ap. J.*, **326**, 368.
Persson, S. E., Frogel, J. A., and Aaronson, M. 1976, *Ap. J.*, **208**, 753.
Pottasch, S. R., Preite-Martinez, A., Olnon, F. M., Jing-Er, M., and Kingma, S. 1986, *Astr. Ap.*, **161**, 363.
Pottasch, S. R., Preite-Martinez, A., Olnon, F. M., Raimond, E., Beintema, D. A., and Habing, H. J. 1985, *Astr. Ap.*, **143**, L11.
Pwa, T. H., Pottasch, S. R., and Mo, J. E. 1986, *Astr. Ap.*, **164**, 184.
Roche, P. F., and Aitken, D. K. 1986, *M.N.R.A.S.*, **221**, 63.
Roche, P. F., Aitken, D. K., and Smith, C. H. 1988, *Ap. J.*, submitted.
Seaton, M. J. 1979, *M.N.R.A.S.*, **187**, 73P.
Sellgren, K., Allamandola, L. J., Bregman, J. D., Werner, M. W., and Wooden, D. H. 1985, *Ap. J.*, **299**, 416.
Tielens, A. G. G. M., and Allamandola, L. J. 1987, in *Interstellar Processes*, ed. D. J. Hollenbach and H. A. Thronson (Dordrecht: Reidel), p. 397.
Tielens, A. G. G. M., Allamandola, L. J., Barker, J. B., and Cohen, M. 1987, in *Polycyclic Aromatic Hydrocarbons and Astrophysics*, ed. A. Leger, L. d'Hendecourt, and N. Boccara (Dordrecht: Reidel), p. 273.
Tokunaga, A. T., Nagata, T., Sellgren, K., Smith, R. G., Onaka, T., Nakada, Y., Sakata, A., and Wada, S. 1988, *Ap. J.*, **328**, 709.
van der Zwet, G. P., and Allamandola, L. J. 1985, *Astr. Ap.*, **146**, 76.
Webster, L., and Glass, I. S. 1974, *M.N.R.A.S.*, **166**, 491.
Witteborn, F. C., and Bregman, J. D. 1984, *Proc. SPIE*, **509**, 123.
Witteborn, F. C., Sanford, S. A., Bregman, J. D., Allamandola, L. J., Wooden, D. H., and Cohen, M. 1988, preprint.
Zeippen, C. J. 1982, *M.N.R.A.S.*, **198**, 111.

L. J. ALLAMANDOLA, J. D. BREGMAN, F. C. WITTEBORN, and D. H. WOODEN: Mailstop 245–6, NASA/Ames Research Center, Moffett Field, CA 94035

M. COHEN: Radio Astronomy Laboratory, 601 Campbell Hall, University of California, Berkeley, CA 94720

M. DE MUIZON: Sterrewacht Leiden, Postbus 9513, NL-2300, RA Leiden, The Netherlands

D. M. RANK: Board of Studies in Astronomy and Astrophysics, Lick Observatory, University of California, Santa Cruz, CA 95064

A. G. G. M. TIELENS: Space Sciences Laboratory, University of California, Berkeley, CA 94720